Design Optimization and Motion Dynamics of Mobility System for Mars Rover

B.Tech. Project: Final Report

Submitted by

Alap Kshirsagar
100100022

Under the Supervision of

Prof. Anirban Guha
Department of Mechanical Engineering
IIT Bombay

DEPARTMENT OF MECHANICAL ENGINEERING
INDIAN INSTITUTE OF TECHNOLOGY BOMBAY

DECLARATION

I Alap Kshirsagar, Roll No.100100022 understand that plagiarism is defined as any one or the combination of the following:

1. Uncredited verbatim copying of individual sentences, paragraphs or illustrations (such as graphs, diagrams, etc.) from any source, published or unpublished, including the internet.

2. Uncredited improper paraphrasing of pages or paragraphs (changing a few words or phrases, or rearranging the original sentence order)

3. Credited verbatim copying of a major portion of a paper (or thesis chapter) without clear delineation of who did or wrote what. (Source: IEEE, The Institute, Dec. 2004)

I have made sure that all the ideas, expressions, graphs, diagrams, etc., that are not a result of my work, are properly credited. Long phrases or sentences that had to be used verbatim from published literature have been clearly identified using quotation marks. I affirm that no portion of my work can be considered as plagiarism and I take full responsibility if such a complaint occurs. I understand fully well that the guide of the seminar report may not be in a position to check for the possibility of such incidences of plagiarism in this body of work.

Signature:

Name:Alap Kshirsagar
Roll No.: 100100022
Date: 07/05/2014

ACCEPTANCE CERTIFICATE

Department of Mechanical Engineering
Indian Institute of Technology, Bombay

This is to certify that **Mr. Alap Ravindra Kshirsagar (100100022)** has satisfactorily completed the B.Tech project entitled **"Design Optimization and Motion Dynamics of Mobility System for Mars Rover"** as a part of the degree of **Bachelor of Technology in Mechanical Engineering** at Indian Institute of Technology, Bombay

Examiner

_____

Supervisor

_____

Chairman

_____

Date: 07/05/2014
Place: IIT Bombay, Powai, Mumbai

Acknowledgements

I would like to express my sincere gratitude towards Prof. Anirban Guha for his mentorship and valuable inputs during the this project. I consider myself very fortunate to be accepted by Prof. Guha to work on this topic under his guidance.

Secondly, this project would not have been successful without the support my team-mates in 'Mars Society India, IIT Bombay'. I would like to thank Aditya Rajgopal, Sai Hemanth, Pranav Bende, Sanket Yadav, Amol Sathawane, Navjeet Kumar for their constant help and contribution in this work. I truly enjoyed working with you guys and will be indebted to you eternally.

Last but certainly not the least, I would like to thank my parents and brother. My family is one of the greatest blessings I have ever been given in life. I could never do enough to sufficiently repay the unconditional love and support they have constantly bestowed upon me.

Alap Kshirsagar

Abstract

Planetary exploration rovers offer promising alternatives for conducting in-situ experiments on earth's neighbour planet -*Mars*. Several configurations have been suggested for the mobility system of such rovers, some of which have been successfully tested in past missions or are being implemented in the upcoming missions. Considering the huge costs of such exploration missions, it becomes necessary to design an optimal mobility system configuration to meet the mission goals. Furthermore given the costs and efforts of building test-beds for evaluating the performance of mobility system and on-board control software, it is also important to develop simulation tools to serve the purpose. The first half of this thesis focuses on obtaining an optimal design configuration of mobility system for mars rover. Various configurations of suspension systems were studied and certain performance metrics were devised to compare their performance. After the preliminary analysis, six-wheel rocker bogie suspension was determined to be most suitable amongst the evaluated configurations. Two performance metrics were considered in the objective funtion for design optimization viz. *Power Consumption* and *Effective Ground Pressure*. Geometric trafficability and load equalization conditions were evaluated to obtain the constraints on design parameters. Analytical expression for driving power was obtained using an established wheel-soil interaction model. The second half of this thesis focuses on development of motion dynamics simulation model for the rocker-bogie suspension system. More recently, researchers have proposed the idea of using reconfigurable wheels, which would be able to change their shape according to the terrain, to improve rover's performance. One of the major challenges in implementation of such wheels is their control and autonomy. To avoid complex on-board calculations, the method of using look-up table for autonomously changing the wheel dimensions is proposed in this thesis. For obtaining this look-up table, a physics based motion dynamics simulation model was developed, incorporating the wheel-soil contact mechanics, drive motor characteristics and motion dynamics of the rocker bogie suspension system. This model was implemented in MATLAB and the simulated motion of rocker bogie system was shown for some test cases. This simulated motion of rocker bogie was found to be in conformance with the ground profile. Another important performance metric called as 'Slip Ratio' was evaluated through the motion simulations. Finally, a lookup table for autonomous shape changing wheels was developed for certain terrain characteristics.

Contents

List of Figures

List of Tables

Chapter 1

Introduction

1.1 Motivation and Objectives

In this age of space technology, robotic exploration of solar system has been at the forefront of various space agencies in the world. Moon and Mars have been particularly focused because of their proximity to earth. This century witnessed one of the greatest achievements of mankind and an engineering marvel in the form of Mars Science Laboratory mission of NASA which successfully landed the truck-sized Curiosity rover on Mars. China showcased its technological capabilities by sending it's first lunar rover 'Jade Rabbit', which unfortunately suffered mechanical failures during hibernation in the extreme cold of lunar night. Indian Space Research Organization is also working on developing a rover for its next moon mission, Chandrayaan-2.

The idea of sending a rover to the surface of another planet is to allow earth bound scientists to access specific areas of interest without enduring the harsh environments of space [1]. The mobility system of rover enables it to carry scientific instruments to various terrestrial formations for in-situ experimentation. Different types of mobility systems have been proposed in the literature. Some of them have been implemented and tested in the form of prototypes or on actual mission rovers. A student group has been formed at IIT Bombay called the 'Mars Society India' to promote research in space technology at undergraduate level. The first activity of this group focuses on building a mars rover prototype to develop expertise in the field of planetary rovers in upcoming years. The author is currently leading the mechanical subsystem of this group and the objectives of this thesis are greatly influenced by the activity. The first objective of this thesis is to select the most suitable mobility system configuration for mars rover. This objective will be accomplished by evaluating the performance of various mobility systems based on certain performance metrics.

The performance of a mobility system is affected to a great extent by its design parameters. Therefore it is important to obtain optimum design parameters to improve rover's performance. This is the second objective of this thesis. It will be accomplished by developing analytical relations between the performance metrics and design parameters of the selected mobility system. Then based on the specific mission objectives, in terms of terrain characteristics and design limitations, optimum design parameters will be obtained.

The development and testing of on-board software for planetary rovers has traditionally

been done using rover hardware platforms and testbeds. These hardware resources are expensive and typically over-subscribed. To alleviate this situation, the need for physics based motion simulation models for planetary rovers arises [10]. Another important application of these simulation tools is in developing and testing new rover technologies such as autonomous control of re-configurable wheels and slip based traction control techniques. Re-configurable wheels or shape changing wheels can improve the performance of rover by adjusting their shape based on the terrain characteristics. To develop autonomous control technique for such wheels, we propose the use of look-up tables which can be fed to the on-board controller. The look up tables will be developed using the dynamic simulation tool for some test scenarios. Thus the next and final objectives of this thesis are to initiate the development of a motion dynamics simulation tool for the selected mobility system and to develop look-up tables for autonomous control of shape changing wheels. These will be accomplished by developing a dynamic simulation model considering the characteristics of wheel actuators, wheel-soil interaction mechanics and motion dynamics of the selected mobility system.

Thus the objectives of this thesis are summarized as:

1. Select the most suitable mobility system for mars rover
2. Optimize the design parameters of selected mobility system based on devised performance metrics
3. Develop terramechanics based motion dynamics simulation tool for the selected mobility system
4. Develop look-up tables for autonomous control of re-configurable wheels

The thesis is organized into 5 chapters. This chapter has outlined the objectives of this thesis. Chapter 2 will present the review of mobility systems and their performance evaluation. Chapter 3 will describe the design optimization procedure for the selected mobility system. Chapter 4 will focus on development of the dynamic simulation tool and application of the simulation results for developing look up table for autonomous re-configurable wheels. Chapter 5 will include the conclusion and scope for future work.

Chapter 2

Performance Evaluation of Mobility Systems

2.1 Review of Mobility Systems for Planetary Rovers

A detailed literature review was carried out to study different types of mobility systems for ground vehicles. The two most common systems are: 4 wheeled systems and 6 wheeled systems. But the tautology does not end there, as each of these systems can be divided into different categories depending on how the wheels are connected to the chassis or to each other.

In an independent suspension system such as spring suspension and legged suspension each of the wheels or limbs are able to move, as the name suggests, independent of each other. In dependent suspension systems the wheels are connected so that they can move in a desired relation to each other. Some common examples of this are rocker-bogie mechanism and articulated suspension. A detailed description of each of these mobility systems is presented below.

2.1.1 Four Wheeled Types

Independent Spring Suspension

Independent suspension is a broad term for any suspension system that allows each wheel on the same axle to move vertically (i.e. reacting to a bump in the road) independent of each other. The Apollo 15 lunar roving vehicle (1971) had this type of suspension system. A four wheeled rover uses a skid steering or Ackerman steering mechanism. Fewer motors are required and the suspension consumes less mass and volume, thereby leaving room for more instruments and power devices. Typically a 4-wheel suspension cannot surmount an obstacle that is larger than its wheel's radius as the rear wheel does not have enough traction [1]. Fig.2.1 shows the 4 wheeled independent spring suspension.

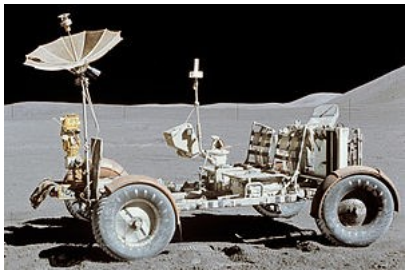

Figure 2.1: Apollo 15 Lunar Rover and 4 wheeled independent spring suspension

Rocker Dependent Suspension

The 4 wheeled rocker dependent system consists of one pair of wheels on each side of the rover that are connected to each other via a passive gear differential to increase the stability of the rover. The suspension itself lifts the body above the wheels creating a large amount of ground clearance. Fig.2.2 shows the 4 wheel rocker dependent suspension.

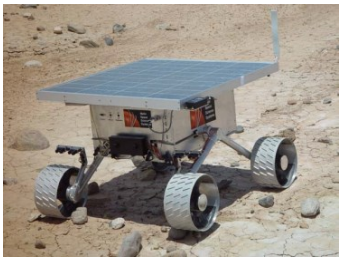

Figure 2.2: ECA lunar rover [Courtesy: Team Indus] and Four wheeled rover II model [1]

Articulated Body Suspension

In articulated body suspension, the left and right pairs of wheels are connected to their own respective body segments. The two bodies are connected together with a free pivot that keeps all four wheels in contact on the ground at all times. The pivot axis is parallel to the wheel axles through the center of the rover. "Ratler" rover designed at Sandia National Labs used this type of suspension. Four wheeled articulated body suspension allows for a simplified drive train and low motor count by using skid steering which simplifies the overall design. But, the limited ground clearance is a major drawback which keeps these rovers from climbing large obstacles. Fig.2.3 shows the 4 wheel articulated body suspension [1].

Figure 2.3: 'Ratler' [Courtesy: Sandia Labs] and 'Nomad' rover [Courtesy: NASA/JPL]

2.1.2 Six wheel types

Independent Spring Suspension

It is similar to the 4-wheel Independent spring suspension, with one extra wheel on each side. It is used in some All-Terrain Vehicles and robotic platforms.

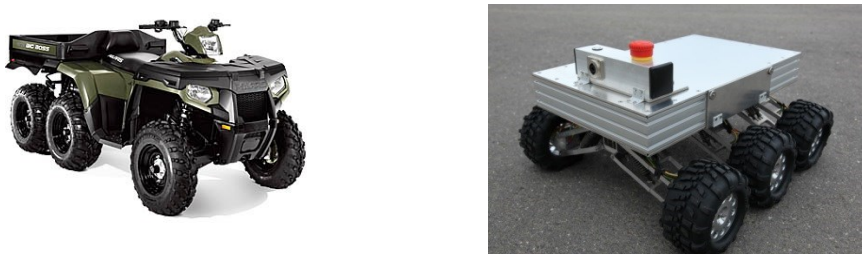

Figure 2.4: Six wheel independent spring suspension in All Terrain Vehicles and Robots

Articulated Body Suspension

The articulated body rover has multiple body segments with a pair of drive wheels under each. The centre axle is a passive hinge to allow all six wheels contact with the ground on uneven terrain. The Surveyor Lunar Rover Vehicle (SLRV) designed by General Motors and the Planetary Rover Test bed Robby are six wheeled articulated body rovers developed for NASA. Theoretically they have the capability to traverse obstacles 50% larger than a wheel diameter but during field tests Robby had difficulty driving over obstacles half a wheel radius high. It was limited by an insufficient amount of wheel torque from the drive train. The SLRV is able to climb steep slopes due to the large contact area from all six wheels but sometimes got hung up in areas of medium sized rocks due to its low ground clearance [11]

Rocker Bogie Suspension

The term "rocker" comes from the design of the differential, which keeps the rover body balanced, enabling it to "rock" up or down depending on the various positions of the multiple wheels. The term bogie refers to the links that have a drive wheel at each end. All three rovers that have successfully carried out mars exploration have a six-wheel rocker bogie suspension

Figure 2.5: 'Blue' rover [Courtesy: NASA/JPL] and 'Robby' rover [Courtesy: NASA/JPL]

system. The rocker-bogie suspension mechanism, along with a differential, enables a six-wheeled vehicle to passively keep all six wheels in contact with a surface even when driving on severely uneven terrain [12] Also it enables the rover to surmount obstacles that are larger than its wheel diameter as it uses an extra set of wheels to provide more forward thrust. However, the system is suitable only at slow speeds of around 10 cm/s, so as to minimize dynamic shocks and consequential damage to the vehicle when surmounting sizable obstacles.

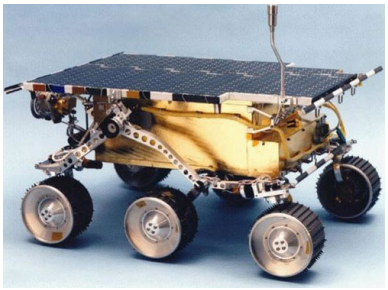

Figure 2.6: 'Curiosity' and 'Sojourner' Mars Rovers [Courtesy: NASA/JPL]

2.1.3 Miscellaneous Types

Inflatable Rover

The general purpose of designing a large, lightweight, inflatable rover is to allow the rover to travel over rocks instead of around them, as most planetary rovers are required to do. This can greatly increase a rover's versatility, speed, and range. The inflatable rover developed by NASA-JPL had three-wheels with a wide wheel base to enhance stability in rugged and steep terrain. The issues with such rovers include complexity, added weight of inflation systems and regulation of temperature of inflation fluid [11]

Legged Robots

Legged robots are usually defined by the number of legs they use. Unlike wheeled rovers, they don't require continuous terrain and can isolate the body from terrain. A lot of research has gone into the gait design and stability of these robots. Still the current level of technology is

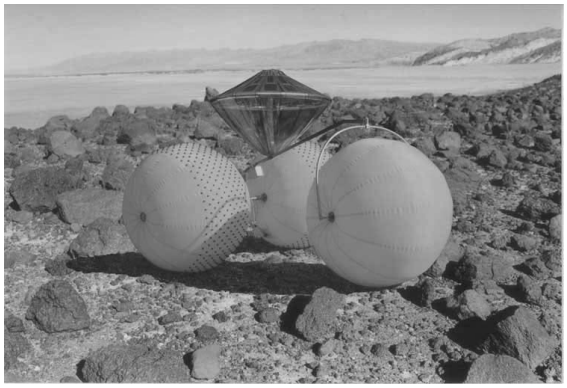

Figure 2.7: Inflatable rover [Courtesy: NASA/JPL]

inadequate for their smooth functioning on unstructured terrain. The major issues are large power consumption and complexity [1]

Figure 2.8: 'Atilla' robot [Courtesy: MIT AI lab] and 'Qrio' humanoid [Courtesy: Sony corp.]

2.2 Performance Evaluation Metrics

Numerous metrics have been proposed and used in literature such as mass, volume, system complexity, power consumption, terrain traversing capability, traction, toppling stability etc.[13] Metrics provide means to assign numerical values to a system's capabilities. Consequently, they allow for an objective comparison of similar systems. The important ones can be determined based on the requirements of a project.

This work focuses on design of mobility system for mars rover. Martian terrain is extremely uneven and the rover is expected to encounter obstacles of 20cm height in the form of small boulders[12]. Power consumption is also an important factor as it has direct impact on the choice of electronic components and energy source. Effective ground pressure, which is a measure of average pressure exerted by wheel on ground, is important as the rover has to be designed to safely operate on soft terrain. Slip ratio is another important metric which

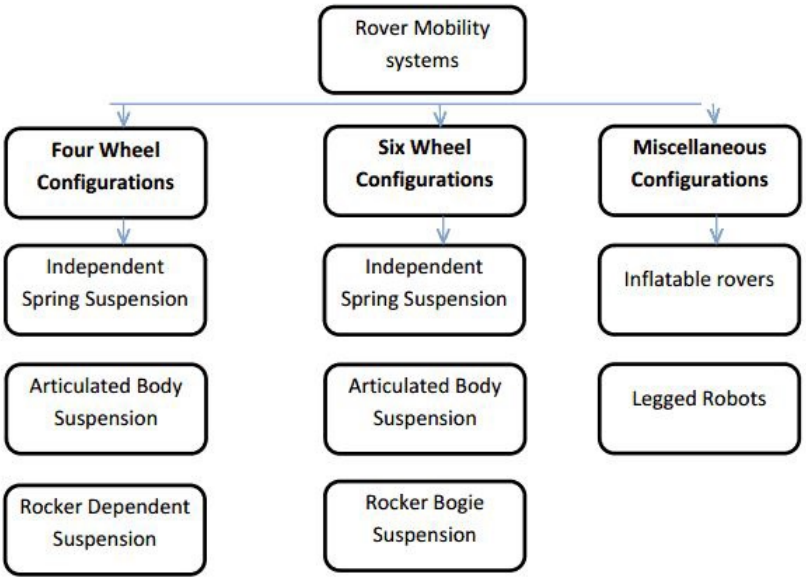

Figure 2.9: Mobility Systems in Planetary Rovers

determines the terrain negotiability of the rover. However slip ratio depends on the terrain under consideration and the motion dynamics of the rover. Thus the analytical evaluation of slip ratio of different mobility systems is not possible and hence slip ratio is not considered for comparing different mobility systems in this work. So following metrics have been selected for performance evaluation of mobility systems which were listed in previous section.

1. Obstacle Negotiability
2. Power Consumption
3. Effective Ground Pressure

Since the exercise in this section is aimed at selecting the most suitable configuration amongst the candidates listed in previous section, preliminary analysis consisting of simplified models and intuitive thought process is presented. The configurations are assigned relative scores for each performance metric on a scale of 1 to 10, with 10 indicating the best candidate. The overall score is calculated by taking the total of individual scores. Legged robots are excluded from the evaluation as they are not suitable for smooth functioning on uneven terrain at the current level of technology. Also inflatable rovers are excluded due to the issues such as complexity, added weight of inflation systems and regulation of inflation fluid temperature[11].

2.2.1 Obstacle Negotiability

Obstacle negotiability is evaluated in terms of driving torque required for climbing a vertical step, with lower value of required torque indicating better performance.

Preliminary Analysis

Keeping the weight, centre of mass, velocity and ground clearance constant, we can compare the maximum driving torque required in each configuration to climb a step of given height. At any given time during climbing a vertical step, the six-wheeled system has at least four wheels that are providing a forward thrust, whereas in case of a 4-wheeled system this number is reduced to two. This leads us to the conclusion that in the six-wheeled system each motor requires less torque compared to the four-wheel system as the total forward thrust required is the same in both cases. Therefore, in terms of obstacle negotiability six-wheeled system has an upper hand.

Furthermore, in a dependent suspension system (i.e. rocker bogie or articulated systems) if any one of the wheels' normal reaction force decreases while climbing an obstacle, it is compensated by an increase in the normal force on another wheel. This is not the case in an independent system. Therefore in terms of obstacle negotiability a dependent suspension system is better than an independent one. Also, in the 6-wheeled independent suspension system, while traversing an obstacle, the front wheels that have already traversed the obstacle might lose contact with the ground, when the middle wheels are climbing. So its obstacle negotiability is restricted further.

Table 2.1: Relative scores based on obstacle negotiability analysis

6 wheel rocker	6 wheel articulated	6 wheel independent	4 wheel rocker	4 wheel articulated	4 wheel independent
10	10	6	5	5	4

2.2.2 Power Consumption

Driving power is the expressed as the product of torque applied by motor and the average angular velocity. Specific power is obtained by dividing the driving power with payload weight. Lower specific power indicates better performance.

Preliminary Analysis

If the payload weight and the average velocity of rover is assumed to be constant, the six-wheeled system has higher mass, owing to the additional wheels and hence is found to have a lower energy efficiency.
W_o = Total weight ; W_p = Payload weight ; W_m = Motor weight ; W_w = Wheel weight ;
τ = Motor torque ; ω = Angular speed of motor
For a 4-wheel system: $W_o = W_p + 4 \times (W_m + W_w)$
For a 6-wheel system: $W_o = W_p + 6 \times (W_m + W_w)$
Assuming that the driving torque requirement for each motor is proportional to the total weight:
$\tau = k * W_o$
Power $= \tau * \omega$, where ω is the angular velocity
Specific Power for 4-wheel system $= 1 + 4 \times \frac{W_w + W_m}{W_p}$

Specific Power for 6-wheel system $= 1 + 6 \times \frac{W_w + W_m}{W_p}$
Therefore the energy efficiency for a 6 wheeled system is lower than the 4 wheeled system.

Table 2.2: Relative scores based on power consumption analysis

6 wheel rocker	6 wheel articulated	6 wheel independent	4 wheel rocker	4 wheel articulated	4 wheel independent
8	8	8	10	10	10

2.2.3 Effective Ground Pressure

Effective ground pressure (EGP) is defined as the average pressure under the average wheel. The average weight on a wheel is first found by dividing the total vehicle weight on a planetary body by the number of wheels. The EGP is found by dividing the average weight by the cross sectional area of the wheel's contact patch on the ground plane[14]. Lower EGP indicates better performance, as it reduces the chances of rover getting stuck in soft terrain.

Preliminary Analysis

If the payload weight and the contact patch area of wheel on ground plane is assumed to be constant, the six-wheeled system has lower average weight on each wheel, owing to the additional two wheels and hence is found to have a lower EGP.

W_o = Total weight ; W_p = Payload weight ; W_m = Motor weight ; W_w = Wheel weight
A = Contact patch area of wheel on ground plane

For a 4-wheel system: $W_o = W_p + 4 \times (W_m + W_w)$
For a 6-wheel system: $W_o = W_p + 6 \times (W_m + W_w)$

EGP for 4-wheel system $= \frac{W_p}{4A} + \frac{W_w + W_m}{A}$

EGP for 6-wheel system $= \frac{W_p}{6A} + \frac{W_w + W_m}{A}$

Therefore the EGP for a 6-wheel system is lower than that for 4-wheel system.

Table 2.3: Relative scores based on power consumption analysis

6 wheel rocker	6 wheel articulated	6 wheel independent	4 wheel rocker	4 wheel articulated	4 wheel independent
10	10	10	7	7	7

Table 2.4: Overall scores

	Obstacle Negotiability	Power Consumption	Effective Ground Pressure	Total Score
4 wheel independent	4	10	7	21
4 wheel articulated	5	10	7	22
4 wheel rocker	5	10	7	22
6 wheel independent	6	8	10	24
6 wheel articulated	10	8	10	28
6 wheel rocker	10	8	10	28

2.3 Conclusion

It can be seen that 6-wheel rocker bogie and 6-wheel articulated mechanisms have highest overall score. Theoretically the articulated system has the capability to traverse obstacles 50% larger than a wheel diameter but during field tests conducted by NASA it had difficulty driving over obstacles half a wheel radius high because of low ground clearance [1]. Furthermore, the 6-wheel articulated system has a segmented chassis which is not desirable for mounting instruments and payloads. Therefore we conclude that the 6-wheel rocker bogie suspension is the best amongst evaluated systems.

Chapter 3

Rocker Bogie Design Optimization

3.1 Rocker Bogie Mechanism

The rocker-bogie suspension system was first used for the mars rover *Sojourner* and is currently NASA's favoured design for rover's mobility system. It has a symmetric structure on both sides of the rover's chassis and a total of six wheels, three on each side. Each side of the suspension has two links, a main rocker and a forward bogie. A wheel and steering mechanism is attached to one end of the main rocker. The opposite end is connected to the forward bogie through a passive pivot joint. A steering mechanism is attached to each end of the forward bogie with the pivot mounted in-between. The two sides of the suspension are connected to a single body from a point on each main rocker. Since rocker bogie is a passive suspension system, it does not have any springs or dampers.

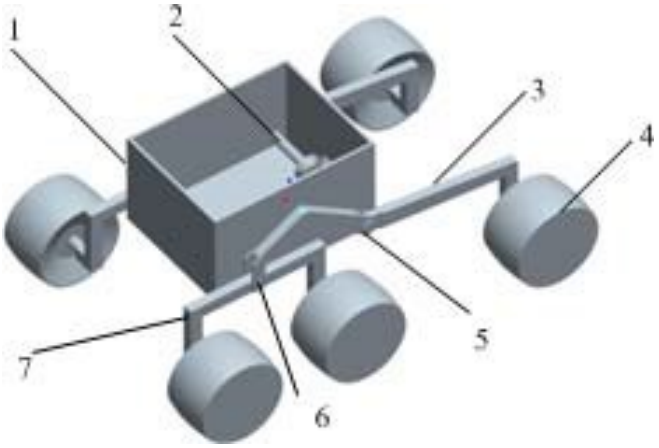

Figure 3.1: 3D model of rocker bogie system[2]

1 Main body; 2- Differential device; 3-Rocker; 4-Wheel
5-Differential Pivot; 6-Free Pivot; 7-Bogie

3.1.1 Mechanical Differential

The main feature of rocker bogie system is the mechanical differential mechanism, which performs the function of pitch averaging. Most commonly used approaches for achieving this feature are a. Bevel Gear Assembly b. Differential Bar

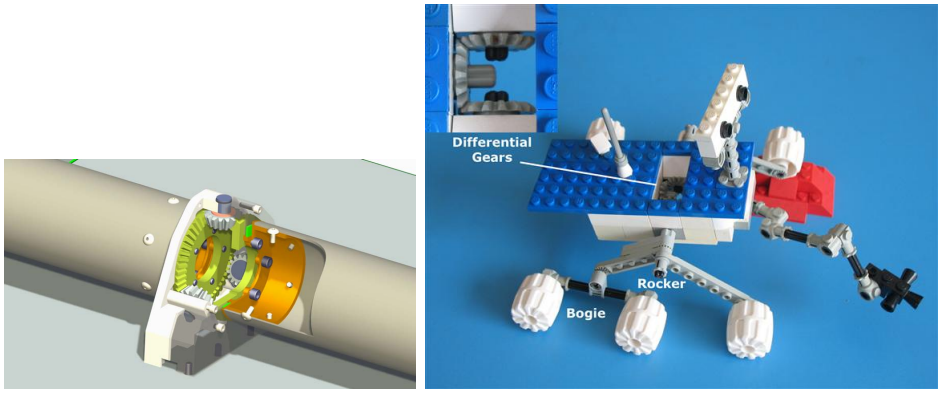

Figure 3.2: Bevel Gear Differential Mechanism [1], [3]

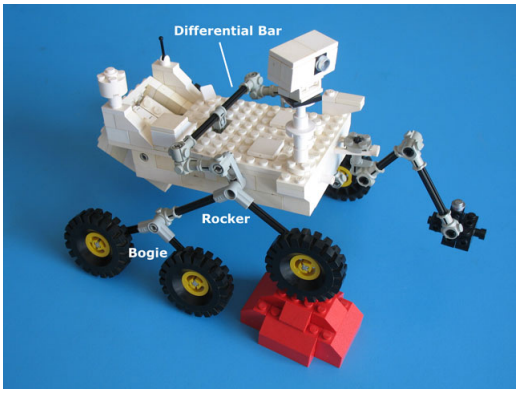

Figure 3.3: Differential bar mechanism [3]

Even though the bevel gear mechanism is compact in construction, it's major drawback is the backlash error in gears. The differential bar mechanism overcomes this problem by replacing gears by mechanical linkages. However in both these mechanisms, the chassis is effectively supported by 3-points of contact with the suspension system. This may lead to chassis instability. In the rover developed by the Mars Society of India-IIT Bombay, which the author is a part of, a novel differential mechanism is implemented.

In this mechanism, as shown in Fig.3.4 the chassis is supported by 4 points of contact: two with the rocker-bogie and two with the differential assembly. The differential mechanism consists of 2 triangular links connected to each other through a member using pin joints. Also the links are connected to the rocker on either side through a member using ball joints. This mechanism ensures that the chassis remains at an average angle of the rocker pitch angles on either side of the rover, while providing 4-point support to the chassis to increase its stability.

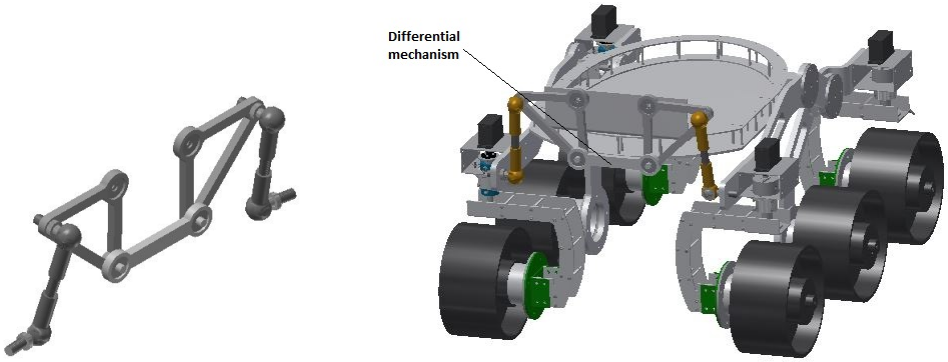

Figure 3.4: Novel Differential Mechanism [Courtesy: Mars Society India, IIT Bombay]

3.1.2 Steering Mechanism

Front and Rear wheels of rocker-bogie suspension system are equipped with independent steering mechanisms. They facilitate the use of Ackerman steering algorithm for smooth turning of the rover. Also the rover is able to turn on-the-spot, allowing it to manuever over challenging terrain. Most common approaches for steering mechanism are: a. Using linear actuators b. Using rotary motors. In some rovers, middle wheels are also equipped with independent steering motors, allowing the rover to traverse both forward/backward and sideways.

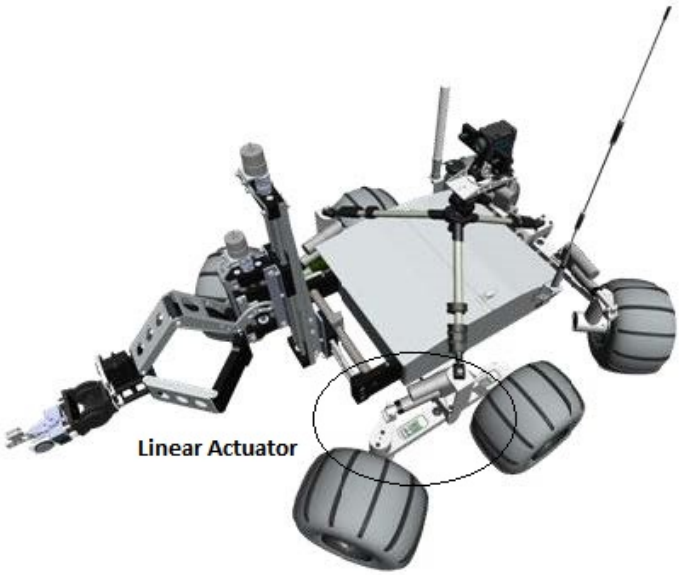

Figure 3.5: Independent Steering Using Linear Actuators [Courtesy: Oregon State University Mars Rover Team]

Figure 3.6: Independent Steering Using Rotary Motors [Courtesy: NASA/JPL]

3.1.3 Design Variables

Two sides of the rover are identical in the rocker-bogie suspension system. Thus for design optimization purpose, we focus only on single side of the rocker-bogie system. In this thesis, following ten parameters are used to define the dimensions of single side of the rocker-bogie system.

Co-ordinates of points A and B : x_a, y_a, x_b, y_b
Co-ordinates of center of mass of rover: x_g, y_g
Radius and width of wheel: r, b
Distances between wheel centers: x_1, x_2

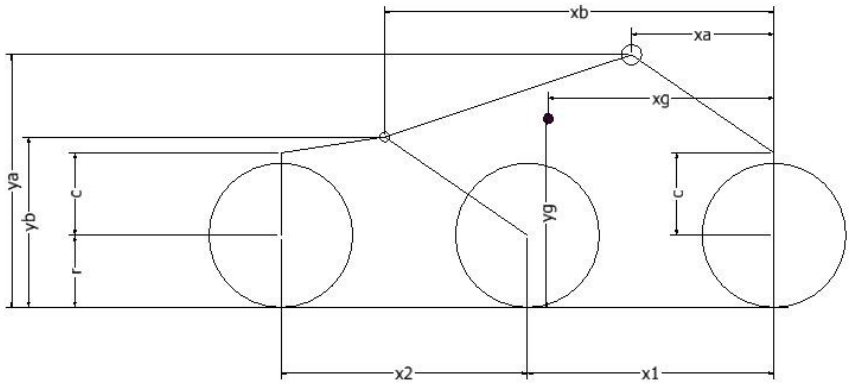

Figure 3.7: Design Variables for Single Side of Rocker-Bogie Suspension System

The parameters are shown in Fig.3.7, where 'c' is the length required for mounting the on-spot turning motors above front and back wheels, which is assumed to be equal to radius of the wheel r to simplify the calculations.

3.2 Evaluation of Performance Metrics

As discussed in Chapter 2, following performance metrics have been selected for design optimization of rocker bogie suspension system:

1. Obstacle Negotiability
2. Power Consumption
3. Effective Ground Pressure

3.2.1 Obstacle Negotiability

Obstacle negotiability of rover depends upon the torque provided by the motor and geometric trafficability constraints. The torque provided by motor is independent of the design parameters. Also, since rocker is much bigger than bogie, the rocker would not interfere with the terrain. However the suspension links of bogie might interfere with the terrain, resulting in loss of mobility of rover. Therefore geometric trafficability analysis of bogie must be carried out. The geometric trafficability of the rover is decided by the terrain geometry and the suspension parameters including the ground clearance of chassis. As shown in figures below, two cases have been analysed:

Case 1: The rover is climbing over a step of height $'h'$, middle and front wheels have successfully climbed over the step and rear wheel has just contacted with the vertical face of barrier.

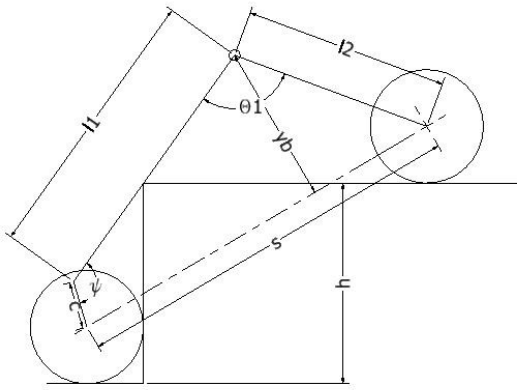

Figure 3.8: Bogie intersecting the vertical step

Substituting the design variables in geometry relations from Fig.3.8,

$$y_b - \frac{h^2 r + r^2 x_2 \sqrt{\frac{x_2^2 - h^2}{x_2^2}} - h r x_b - r x_2 x_b + h x_2 x_b \sqrt{\frac{x_2^2 - h^2}{x_2^2}}}{h^2 + r\sqrt{\frac{x_2^2 - h^2}{x_2^2}}} > 0 \tag{3.1}$$

Case 2: The rover is climbing over an obstacle of height $'h_2'$ and width $'w'$, middle wheel has just overcome the obstacle and landed on horizontal surface.

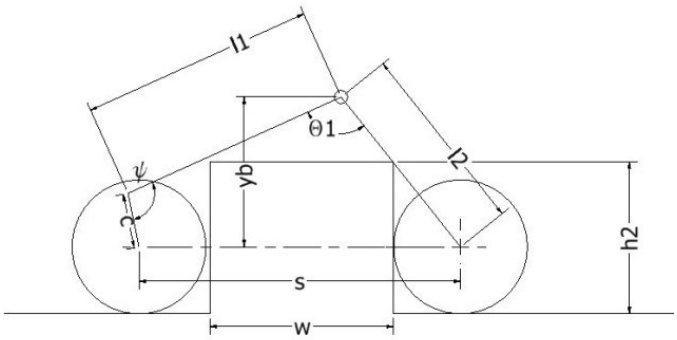

Figure 3.9: Bogie intersecting the obstacle

Substituting the design variables in geometry relations from Fig.3.9,

$$y_b - \frac{(h-r)(x_b - x_1)}{r} - r > 0 \tag{3.2}$$

$$x_2 \geq w + 2r \tag{3.3}$$

Also the ground clearance should be greater than y_b

$$y_a - y_b > 0 \tag{3.4}$$

Thus the equations 3.1, 3.2, 3.3 and 3.4 give the constraints on design parameters for given obstacle dimensions and vertical step height.

3.2.2 Power Consumption

The total power consumption of rover includes the power consumed by driving motors, steering motors and other payloads.

$$P_{total} = N_w \times P_{driving} + N_s \times P_{steering} + P_{payloads} \tag{3.5}$$

where N_w - Number of wheels, N_s - Number of independently steered wheels

Payload power consumption is independent of suspension design parameters, so it is taken as a constant. Steering motors are powered only during turning motion. Assuming the rover is moving along a straight trajectory (no turning), the total power consumption of rover is given by:

$$P_{total} = N_w \times P_{driving} + P_{payloads} \tag{3.6}$$

The power consumption of driving motor is computed as [15]:

$$P_{driving} = \frac{\tau_{wheel} \times \omega_{wheel}}{\eta_{ampli} \times \eta_{motor} \times \eta_{gearbox}} \tag{3.7}$$

$$\tau_{wheel} = R_{total} \times r_{wheel} \tag{3.8}$$

$$\omega_{wheel} = \frac{v_{rover}}{r_{wheel}} \tag{3.9}$$

where τ_{wheel} - Driving motor torque
ω_{wheel} - Wheel angular speed
r_{wheel} - Wheel radius
v_{rover} - Forward speed of rover

The amplifier efficiency η_{ampli} is considered to be constant while the motor and gearhead efficiencies η_{mot} and η_{gear} are functions of different parameters. The motor efficiency is a function of speed, torque and motor type and the gearhead efficiency is a function of gearhead ratio, applied torque and maximal sustainable torque. For simplifying the calculations all efficiencies are assumed to be constant.

In Eq.3.8, the total motion resistance R_{total} is used to compute the wheel torque. It depends upon the wheel dimensions, wheel-soil interaction and terrain conditions. There exist four general wheel-terrain interactions [4]

1. Rigid wheel travelling over rigid terrain
2. Deformable wheel travelling over rigid terrain
3. Rigid wheel travelling over deformable terrain
4. Deformable wheel travelling over deformable terrain

In most of the planetary rovers, wheels are generally metallic and their deflection under static loading is much lower than the deformation of soil/terrain. So the model 'Rigid wheel travelling over deformable terrain' is suitable for this condition. In this model, the rolling resistance is neglected as the deformation of wheel is very small. Motion resistance of tire consists of two major components: the compaction resistance and the bulldozing resistance.

Compaction resistance (R_c), which represents the resistance due to terrain deformation, is given as [16]

$$R_c = \frac{\left(\frac{3W}{\sqrt{D}}\right)^{\frac{2n+2}{2n+1}}}{(3-n)^{\frac{2n+2}{2n+1}} \times (n+1) \times b^{\frac{1}{2n+1}} \times \left(\frac{k_c}{b} + k_f\right)^{\frac{1}{2n+1}}} \tag{3.10}$$

Bulldozing resistance (R_b) is developed when a substantial soil mass is displaced by a wheel. It is given as [16]

$$R_b = b\left(c \times z \times k_{pc} + 0.5 \times z^2 \times \gamma \times k_{py}\right) \tag{3.11}$$

where z is the static sinkage of the wheel given by,

$$z = \left(\frac{3W}{(3-n)\left(k_c + bk_f\right) \times \sqrt{D}}\right)^{\frac{2n}{2n+1}} \tag{3.12}$$

where b - Width of wheel
k_c, k_f, n - Pressure sinkage parameters of the specific terrain

W - Normal load on wheel
D - Wheel Diameter, c - Cohesion
k_{pc}, k_{py} - Terzaghi soil factors
γ -Soil density

Apart from the resistances to motion of wheel, the rover encounters gravitational resistance R_g, while climbing a slope, given as the projection of weight on the slope.

$$R_g = \frac{M_{total}}{N_w} g_{mars} sin\,(\theta) \tag{3.13}$$

where M_{total} - Total mass of rover
g_{mars} - Acceleration due to gravity on mars = 3.711 m/s^2
θ - Slope angle
Total mass of the rover can be estimated as

$$M_{total} = M_{chassis+payload} + N_w\,(M_{wheel} + M_{driving}) + N_s M_{steering} + M_{links} \tag{3.14}$$

$$M_{wheel} = f(r_{wheel}, b) \tag{3.15}$$

$$M_{links} = f(l_1, l_2, l_3, l_4) \tag{3.16}$$

where $M_{payload}$ - Total mass of payload on rover (independent of design parameters)
M_{wheel} - Mass of wheel (function of wheel dimensions)
$M_{driving}$ - Mass of driving motor (independent of design parameters)
$M_{steering}$ - Mass of steering assembly (independent of design parameters)
M_{links} - Mass of suspension links (function of link lengths)
l_1, l_2, l_3, l_4 - Lengths of rocker bogie suspension links

In reality, the mass of chassis, payload and motors will be much greater than the mass of wheels and suspension links. Therefore for simplifying the design optimization calculations, the total mass of rover can be assumed to be independent of design parameters.

3.2.3 Effective Ground Pressure

Effective ground pressure (EGP) is defined as the average pressure under the average wheel. The average weight on a wheel is first found by dividing the total vehicle weight on a planetary body by the number of wheels. The EGP is found by dividing the average weight by the cross sectional area of the wheel's contact patch on the ground plane [14]

$$Averageweightperwheel = \frac{M_{total} g_{mars}}{N_w} \tag{3.17}$$

$$EGP = \frac{M_{total} g_{mars}}{N_w r_{wheel} b} \tag{3.18}$$

where M_{total}- Total mass of rover
g_{mars} - Acceleration due to gravity on mars = 3.711 m/s^2
N_w - Number of wheels
r_{wheel} - Wheel radius
b - Width of wheel

3.3 Design Optimization

In the previous section, the expressions for performance metrics were derived in terms of the design parameters along with the constraints on design parameters. This section presents the optimization procedure for calculating the design parameters.

3.3.1 Optimization Scenario

For simplifying the calculations, the ground profile on which rover is moving is assumed to be flat. Two optimization scenarios are considered: First scenario is based on the design limitations of the University Rover Challenge (URC) competition, as the author is a part of IIT Bombay's Rover Team for this competition. Second optimization scenario is based on the available data of Curiosity rover - *Mars Science Laboratory* mission of NASA, which is currently operating on mars.

Table 3.1: Optimization Scenario

Optimization Scenario	N_w	V_{rover}	η	L_{rover}	W_{rover}	g
1-University Rover Challenge	6	1m/s	0.7	1.2m	50kg	9.81 m/s^2
2-Curiosity Rover, NASA	6	0.01m/s	0.9	3m	900kg	3.8 m/s^2

N_w - Number of independently driven wheels
V_{rover} - Average Velocity of Rover
η - Efficiency of driving motors
L_{rover} - Length of rover
W_{rover} - Weight of rover
g - Acceleration due to gravity

The soil properties for calculation of driving power are based on the results for martian soil simulants [17]

Table 3.2: Soil Properties

γ (kg/m^3)	540	ϕ	29.48
n	0.67	N_c	27.86
k_c (kPa/m^{n-1})	67.28	N_q	16.44
k_f (kPa/m^n)	0.68	N_γ	19.34
Φ (deg)	29.48	k_{pc}	20.68
c (kPa)	1.33	k_{py}	52.61

3.3.2 Power Consumption Analysis

Power consumption was observed to be a function of wheel dimensions. Fig.3.10 and Fig.3.11 show the variation of driving power with wheel radius and wheel width respectively, for both the optimization scenarios.

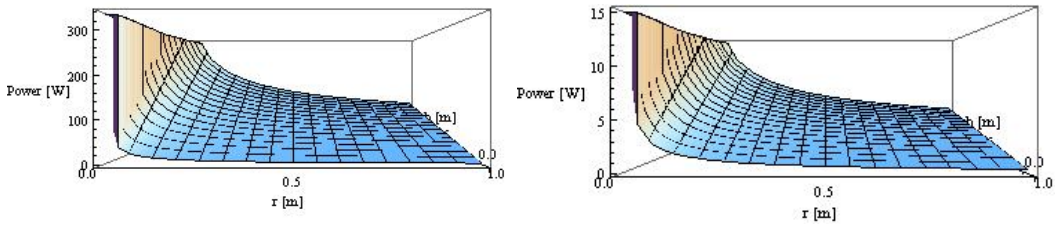

(a) Optimization Scenario 1 (b) Optimization Scenario 2

Figure 3.10: Variation of drive power with wheel radius

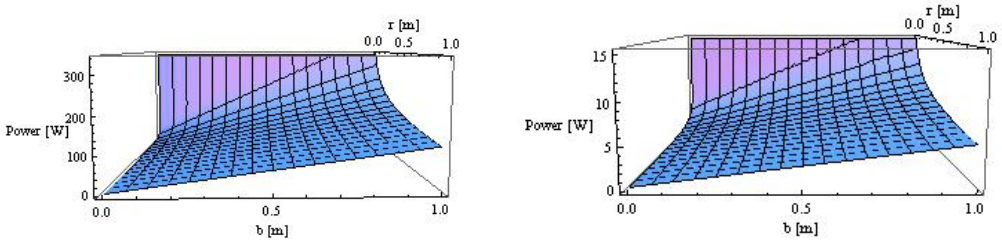

(a) Optimization Scenario 1 (b) Optimization Scenario 2

Figure 3.11: Variation of drive power with wheel width

The power consumption is found to decrease exponentially with increase in wheel radius and increase with increase in wheel width. As the radius of the wheel is increased, the static sinkage decreases as defined in Eq.3.12. Since the soil resistance is directly proportional to the static sinkage, the drive power required to overcome the resistance also decreases with increase in wheel radius. Similarly increase in wheel width increases the soil resistance, resulting in higher required drive power.

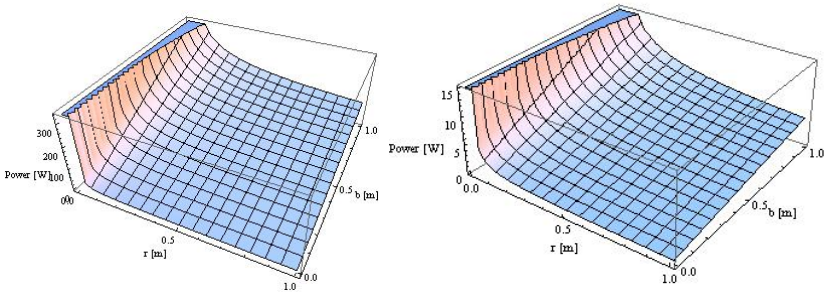

(a) Optimization Scenario 1 (b) Optimization Scenario 2

Figure 3.12: Variation of drive power with wheel dimensions

3.3.3 Effective Ground Pressure Analysis

Effective ground pressure (EGP) is also a function of the wheel dimensions. These graphs show the variation of EGP with wheel radius and wheel width.

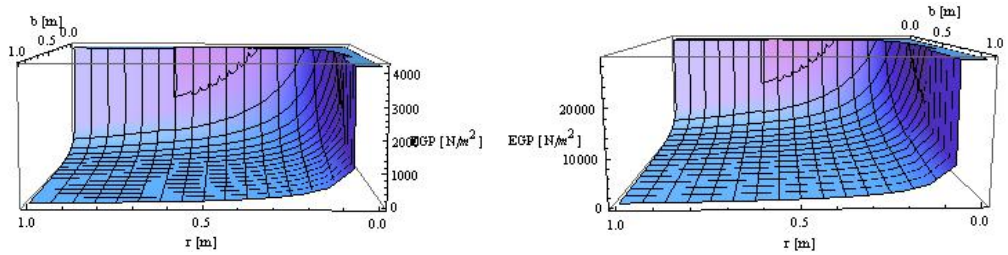

(a) Optimization Scenario 1 (b) Optimization Scenario 2

Figure 3.13: Variation of effective ground pressure with wheel radius

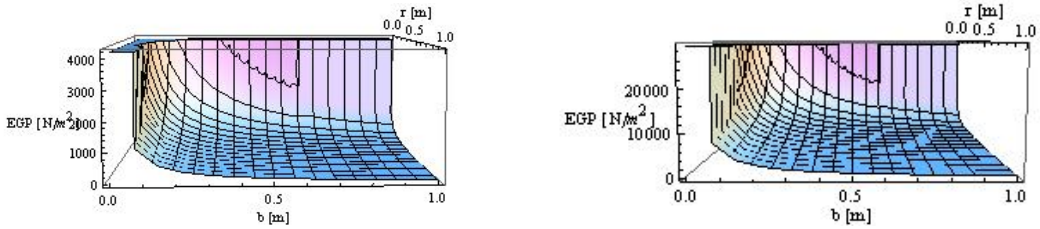

(a) Optimization Scenario 1 (b) Optimization Scenario 2

Figure 3.14: Variation of effective ground pressure with wheel width

So the effective ground pressure decreases with increase in wheel radius and wheel width. As defined in Eq.3.17, effective ground pressure is inversely proportional to the contact patch area. Thus EGP decreases with increase in wheel size.

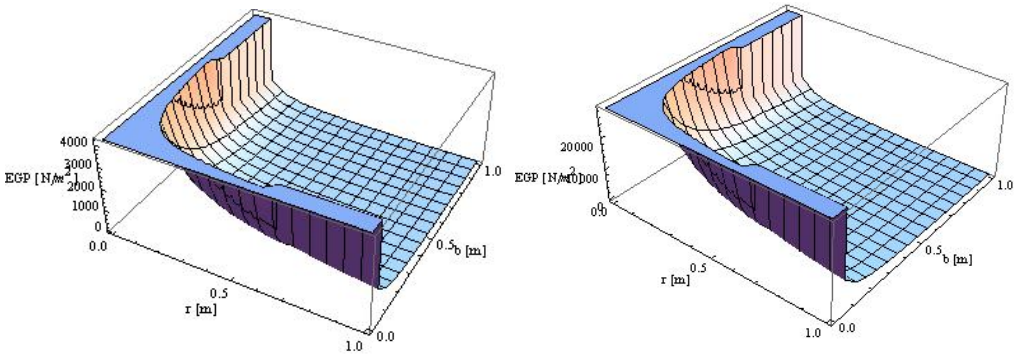

(a) Optimization Scenario 1 (b) Optimization Scenario 2

Figure 3.15: Variation of effective ground pressure with wheel dimensions

3.3.4 Optimization Process

The objective function to be minimized is defined as the weighted sum of power consumption and ground pressure.

$$ObjectiveFunction = \frac{w_1}{w_p} \times PowerConsumption + (1 - w_1) \times \frac{GroundPressure}{w_{egp}} \quad (3.19)$$

From power consumption and EGP analysis, it can be seen that wheels with larger diameter and lower width tend to minimize power consumption. On the other hand, wheels with larger diameter and larger width tend to minimize effective ground pressure on wheels. Thus the value objective function decreases monotonically with increase in wheel radius. However the geometric trafficability constraints given in Eq.3.1, 3.2, 3.3 and 3.4 limit the values of design parameters. More constraints can be derived for static load equalization condition on wheels.

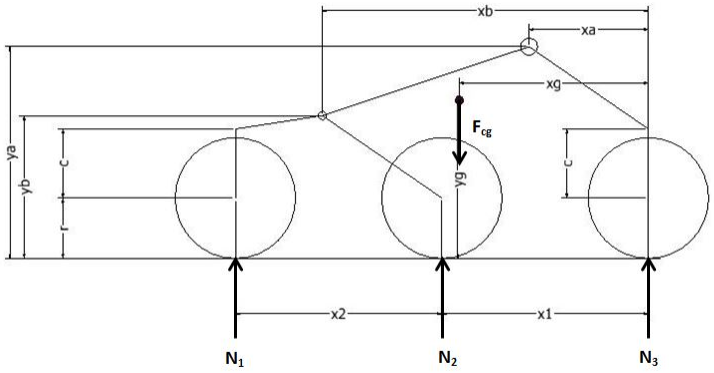

Figure 3.16: Static model of single side of rocker bogie

Load Equalization

Fig.3.16 shows the external forces on single side of rocker bogie on flat ground. The force balance condition along vertical direction is given by:

$$N_1 + N_2 + N_3 = F_{cg} \quad (3.20)$$

Similarly the moment balance condition about the central axis of front wheel is given by:

$$N_1 \times (x_1 + x_2) + N_2 \times x_1 = F_{cg} \times x_{cg} \quad (3.21)$$

Since point B is a free pivot, it cannot transfer axial torque. The moment balance equation of bogie about point B is given by:

$$N_1 \times (x_b - x_1) = N_2 \times (x_1 + x_2 - x_b) \quad (3.22)$$

For load equalization $N_1 = N_2 = N_3$. Substituting this in above equations we obtain following relations between the design parameters:

$$x_b = x_1 + \frac{x_2}{2} \tag{3.23}$$

$$x_{cg} = \frac{2x_1 + x_2}{3} \tag{3.24}$$

The weighing factors w_p and w_{egp} in Eq.3.19 are used to normalize the order of magnitudes of the performance metrics, while the weighing factor w_1 signifies the relative importance of each performance metric in the objective function. The values of w_p and w_{egp} are based on the power consumption analysis and effective ground pressure analysis presented in Section 3.3.2 and 3.3.3. Fig.3.17 shows the variation of objective function with wheel width for different values of w_1.

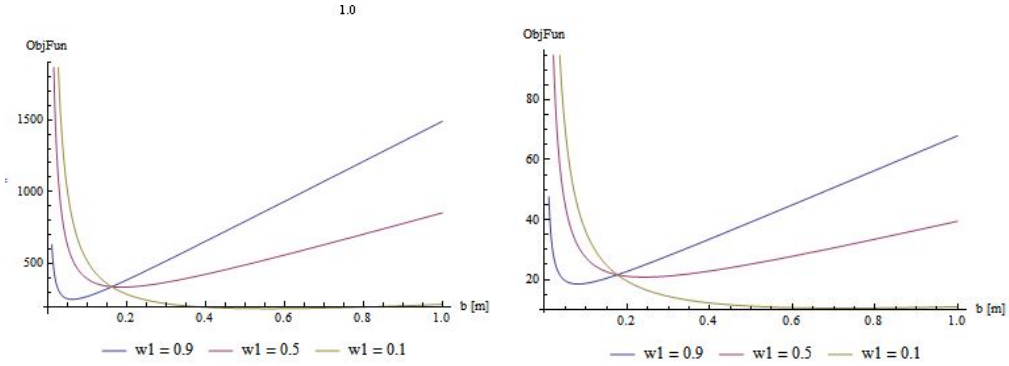

(a) Optimization Scenario 1 (b) Optimization Scenario 2

Figure 3.17: Variation of objective function with wheel diameter for different weighing factors

Thus it can be seen that the optimum values of design variables strongly depend upon the weighing constant w_1. We assume w_1 to be 0.5, which signifies that minimizing power consumption and minimizing ground pressure are given equal importance in the design.

Table 3.3: Weighing factors

Optimization scenario	w_p	w_{egp}	w_1
1	1	10	0.5
2	1	1000	0.5

The constrained global optimization is carried out using 'Nelder Mead' method available in MATHEMATICA. 'Nelder Mead or Downhill simplex method' is a commonly used non-linear optimization technique, which is well defined numerical method for problems for which derivatives may not be known or continuous. Nelder Mead method was chosen because of it's simplicity and inbuilt implementation in MATHEMATICA. The results of optimization are given in Table 3.4 and 3.5.

The procedure for design optimization is summarized in Fig.3.18.

Table 3.4: Optimized design parameters

Scenario	x_1	x_2	r	x_b	x_g	b	x_a	y_a	y_b	y_g
1	0.45	0.45	0.15	0.675	0.45	0.1858	$x_a < 0.45$	$y_a > y_b$	$y_b > 0.375$	-
2	1.125	1.125	0.375	1.8	1.2	0.1859	$x_a < 1.2$	$y_a > y_b$	$y_b > 0.9$	-

Table 3.5: Values of performance metrics for optimized design parameters

Scenario	Driving Power (W)	Effective Ground Pressure (N/m^2)
1	13.40	8176.44
2	374.38	2931.68

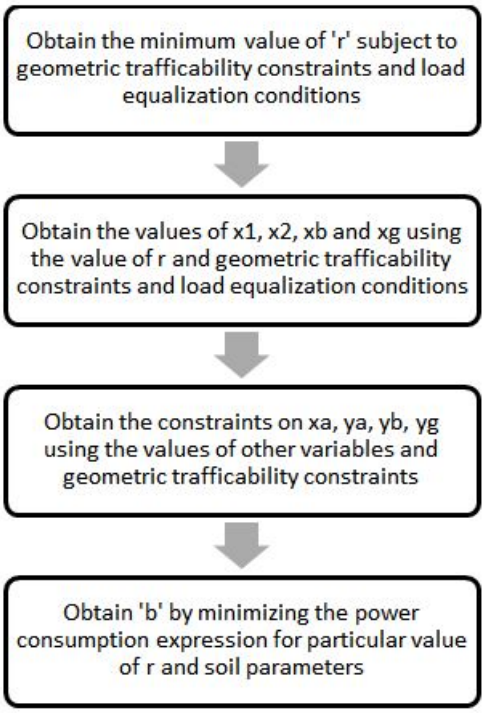

Figure 3.18: Summary of optimization process

Chapter 4

Motion Dynamics Simulation Model for Rocker Bogie Suspension System

4.1 Introduction

The motion of rover on any terrain is influenced by the mobility system configuration, design parameters, actuator characteristics and wheel-soil interaction. Mostly the dynamic effects are neglected in rover simulations owing to their slow speeds and computational complexity in dynamic modelling. However, in future when rovers will be operating alongside human beings, they'll have to operate at much higher speeds. Hence there is a need to develop dynamic simulation models for planetary rovers. As seen in Chapter 2, rocker-bogie suspension system has been found to be most suitable for operation on mars. This chapter focuses on initiating the development of a Motion Dynamics Simulation Tool for the rocker bogie suspension system.

A simplified model consisting of single side of the rocker bogie system is used in this work. However, the model can be extended to full system in the future. We first study the wheel-soil interaction mechanics to obtain the contact forces on wheels. There are well-established terramechanics models for different types of wheel-terrain interactions. In this thesis, a novel method for incorporating the wheel deformation has been proposed. The equations for motion dynamics of the rocker bogie suspension system are developed using articulated body dynamics. A MATLAB program is developed to implement the wheel-terrain contact mechanics and motion dynamics of the rocker bogie suspension system. Currently, only the rigid wheel contact model is incorporated in the simulation tool due to time constraints. The motion of rover is simulated for some test cases. The application of this simulation tool in developing look up tables for autonomous control of re-configurable wheels is also demonstrated.

4.2 Wheel-soil contact model based on Terramechanics approach

When the rover moves over any arbitrary terrain, the normal and tractive forces acting on wheels depend upon the wheel-soil interaction mechanics. The mechanics of interaction between different wheels and terrains has been studied in the field of Terramechanics. The fundamentals of terramechanics were established by M. Bekker in 1960s [18]. Since then there have been many developments in this field including various contact models, simplified stress distributions and different methods for measuring terrain characteristics. Most common wheel-terrain interactions are categorized into four types as shown in Fig.4.1 :
A. Rigid Wheel over Rigid Terrain
B. Deformable Wheel over Rigid Terrain
C. Rigid Wheel over Deformable Terrain
D. Deformable Wheel over Deformable Terrain

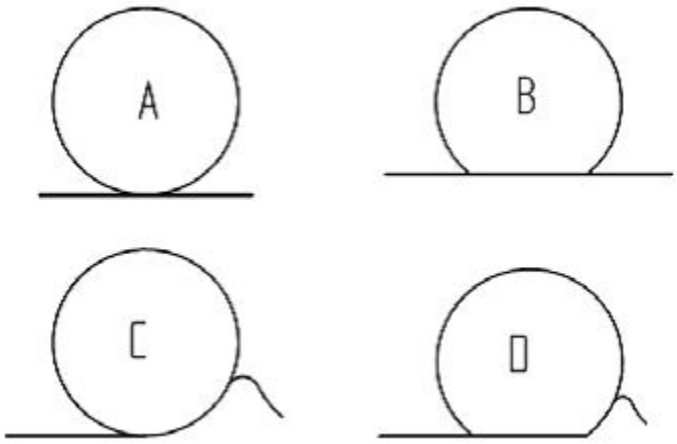

Figure 4.1: Different types of wheel-soil interactions [4] [5]

In case of planetary exploration rovers, wheels are generally metallic and their deflection under static loading is much lower than the deformation of soil/terrain. So the model Rigid Wheel travelling over Deformable Terrain is suitable for this condition. In the future, when rovers will be operating alongside human beings on mars, they can have elastic wheels to to absorb the dynamic loads and provide a smooth ride. Thus the need to develop models for 'Deformable Wheel travelling over Deformable Terrain' arises.

The terramechanics model for 'Rigid Wheel travelling over Deformable Terrain' used in this thesis is similar to the one presented in [6] and [19]. For the deformable wheel case, a new method is proposed to calculate the deformed shape of the wheel. But due to computational limitations and time constraints, this method is not incorporated in the dynamic simulation tool developed as a part of this thesis. In future, deformable wheel case can be included in the simulation tool.

4.2.1 Contact model for rigid wheel over deformable terrain

Slip Ratio

Slip ratio is a key variable to evaluate the mobility performance of the rover. It is also used to calculate the wheel-terrain contact forces. Slips are generally observed when a rover travels on loose soil. The slip in the longitudinal direction is expressed by the slip ratio s, which is defined as a function of the longitudinal travelling velocity of the wheel v and the circumference velocity of the wheel $r\omega$, where r is the wheel radius and ω represents the angular velocity of the wheel.

$$s = \begin{cases} \frac{r\omega - v}{r\omega} & : |r\omega| > v \quad (accelerating) \\ \frac{r\omega - v}{v} & : |r\omega| < v \quad (decelerating) \end{cases} \tag{4.1}$$

The slip ratio assumes a value in the range from -1 to 1. When the slip ratio is -1 or 1, it indicates that the wheel has stopped moving forward/backward and is slipping in its place. When the slip ratio is zero, then it indicates the pure rolling motion.

Static Wheel Sinkage

When the rover is stationary, vertical load on each wheel determines its static sinkage. According to the equation formulated by Bekker [18], the static stress p_h generated under a flat plate, which has a sinkage h and width b is calculated as follows:

$$p(h) = \left(\frac{k_c}{b} + k_{phi} \right) h^n \tag{4.2}$$

where k_c and k_{phi} represent pressure sinkage modules and n is the sinkage exponent. As shown in Fig.4.2, for a rigid wheel over deformable terrain, the following formulae can be derived. First, the wheel sinkage $h(\theta)$ at an arbitrary angle θ is geometrically given by the following relation:

$$h(\theta) = r(cos\theta - cos\theta_s) \tag{4.3}$$

where θ_s is the static contact angle.

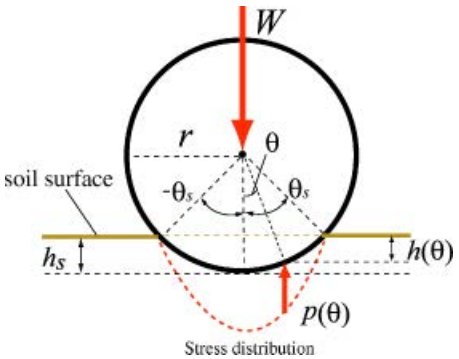

Figure 4.2: Static sinkage for rigid wheel over deformable terrain [6]

Substituting the Eq.4.3 into Eq. 4.2 we obtain the variation of pressure p with θ:

$$p(\theta) = r^n \left(\frac{k_c}{b} + k_{phi} \right) (cos\theta - cos\theta_s)^n \tag{4.4}$$

The static contact angle θ_s is numerically obtained by solving the following equation when the vertical load W is known:

$$W = \int_{-\theta_s}^{\theta_s} p(\theta) br cos\theta d\theta = r^{n+1}(k_c + k_{phi} b) \times \int_{-\theta_s}^{\theta_s} (cos\theta - cos\theta_s)^n cos\theta d\theta \tag{4.5}$$

Finally the static sinkage h_s is derived as follows:

$$h_s = r(1 - cos\theta_s) \tag{4.6}$$

Wheel Contact Angles and Stress Distribution for Rotating Wheel

Fig.4.3 shows the model of a rotating rigid wheel on deformable terrain. The angle from the vertical to the point where the wheel initially makes contact with the soil is defined as the forward angle θ_f. Similarly the angle from the vertical to the point where the wheel departs from the soil is defined as the rear angle θ_r. The wheel contact patch on loose soil is defined by the region from θ_f to θ_r.

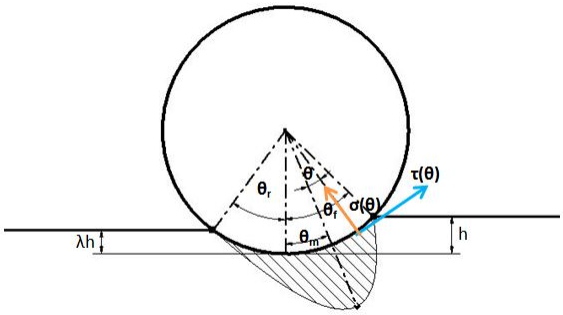

Figure 4.3: Wheel contact angle and Stress model

As shown in Fig.4.3, the entry angle θ_f is expressed as a function of h:

$$\theta_f = cos^{-1} \left(1 - \frac{h}{r} \right) \tag{4.7}$$

The exit angle θ_r is modelled by using the wheel sinkage ratio λ, which denotes the ratio between the front and the rear sinkages of the wheel.

$$\theta_r = cos^{-1} \left(1 - \frac{\lambda h}{r} \right) \tag{4.8}$$

The value of λ depends on the soil characteristics, wheel surface pattern, and slip ratio. It decreases below 1.0 when soil compaction occurs, but can be greater than 1.0 when the soil

is dug by the wheel and transported to the region behind the wheel. The value of λ is 1 when the slip ratio is zero and wheel is placed over flat terrain.

The stress field below the wheel can be divided into two parts: normal stress distribution and shear stress distribution. The normal stress distribution is determined by the following equation [20]:

$$\sigma(\theta) = \begin{cases} r^n \left(\frac{k_c}{b} + k_{phi}\right) \left[cos\theta - cos\theta_f\right]^n & : \theta_m \leq \theta < \theta_f \\ r^n \left(\frac{k_c}{b} + k_{phi}\right) \left[cos\left(\theta_f - \frac{\theta - \theta_r}{\theta_m - \theta_r}(\theta_f - \theta_m)\right) - cos\theta_f\right]^n & : \theta_r < \theta \leq \theta_m \end{cases} \tag{4.9}$$

The normal stress is maximized at a specific angle θ_m given by:

$$\theta_m = (a_0 + a_1 s)\theta_f \tag{4.10}$$

where a_0 and a_1 are parameters that depend on the wheel-soil interaction. Their values are generally assumed as $a_0 \approx 0.4$ and $0 \leq a_1 \leq 0.3$ [21]

The shear stress distribution $\tau(\theta)$ is given by [16]:

$$\tau(\theta) = (c + \sigma(\theta) tan\phi) \left[1 - e^{\frac{r}{k}\left[\theta_f - \theta - (1-s)(sin\theta_f - sin\theta)\right]}\right] \tag{4.11}$$

where c represents the cohesion stress of the soil, ϕ is the internal friction angle of the soil, k is the shear deformation module.

Resultant Forces and Torque

The normal and shear stress distributions below the wheel can be converted into resultant forces and torque acting at the wheel center. The net force in x-direction is called as the 'Drawbar Pull'. The expression for drawbar pull is obtained from the $\sigma(\theta)$ and $\tau(\theta)$ expressions [21]:

$$F_x = rb \int_{\theta_r}^{\theta_f} \left[\tau(\theta) cos\theta - \sigma(\theta) sin\theta\right] d\theta \tag{4.12}$$

The net-force in y-direction is called as the 'Vertical Force' and is obtained by the same method as described in Eq.4.12 [21]

$$F_y = rb \int_{\theta_r}^{\theta_f} \left[\tau(\theta) sin\theta + \sigma(\theta) cos\theta\right] d\theta \tag{4.13}$$

The shear stress distribution results in a net torque about the axis of rotation of the wheel passing through the wheel center. The expression for this torque is derived as:

$$T = r^2 b \int_{\theta_r}^{\theta_f} \tau(\theta) d\theta \tag{4.14}$$

4.2.2 Contact Model for Deformable Wheel over Deformable Terrain

Deformed Shape of Wheel

In case of a deformable wheel, there is a change in the shape of wheel's portion in contact with the ground. Some approaches have been proposed in the literature for modeling the deformed shape of the wheel. The most classical approach is proposed by Bekker and implemented in [22]. This model uses a larger substitute circle to describe the deformed contact patch between tyre and soil. The diameter of the substitute circle is calculated from the equilibrium between the vertical reaction force of the soil and the vertical load on the tyre. The equilibrium equation is solved by iteration procedure. In[5] the deflected area of the wheel is assumed to be flat and the deflection is calculated by a similar iterative procedure involving calculation of vertical soil force and equating it with the vertical load on wheel. Both the approaches mentioned above assume some simplified shape for the deflected portion

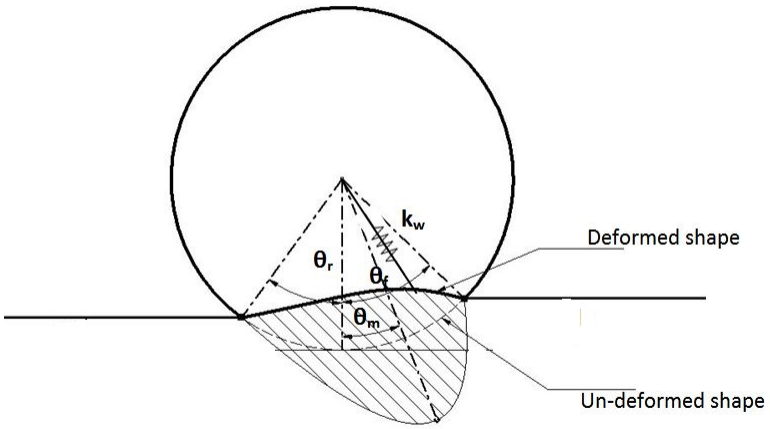

Figure 4.4: Deformable wheel travelling over deformable terrain model

of the wheel. In this thesis, we propose a new model for obtaining the deformed shape of the wheel. Fig.4.4 shows the schematic of deformable wheel travelling over deformable terrain. We consider a small section of the deformed profile as shown in Fig.4.5

In this model, we assume the stiffness of the wheel to be k_w per unit surface area. This can be calculated experimentally using load tests. The normal stress and shear stress at any θ will be along the tangent to the surface at that point. The slope of the tangent to the surface is given by:

$$tan\alpha = \frac{rsin\theta - \frac{dr}{d\theta}cos\theta}{rcos\theta + \frac{dr}{d\theta}sin\theta} \tag{4.15}$$

The spring force is given by:

$$F_{spring} = k_w[r(\theta) - r_0]\delta A \tag{4.16}$$

The resultant of all the forces along the perpendicular direction to the surface normal should be zero for equilibrium condition. The force balance equation results in the following ex-

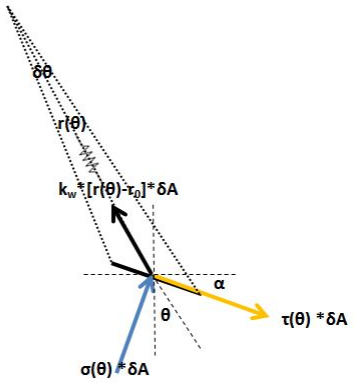

Figure 4.5: Forces on small element of deformed wheel

pression:

$$k_w[r(\theta) - r_0] = \sigma(\theta)cos(\alpha - \theta) + \tau(\theta)sin(\alpha - \theta) \tag{4.17}$$

where r_0 is the initial radius of the wheel, $\sigma(\theta)$ is the normal stress given in Eq.4.9, $\tau(\theta)$ is the shear stress given in Eq.4.20. The above equation can be solved numerically to obtain the deformed shape of the wheel.

Static Wheel Sinkage

The static sinkage in case of deformable wheel is given by:

$$h_s = r(0) - r_0 * cos\theta_f \tag{4.18}$$

where $r(0)$ is the radius at $\theta = 0$ in the deformed shape, r_0 is the un-deformed wheel radius, θ_f is the forward contact angle.

Stress Distribution for Rotating Deformable Wheel

Stress distribution below a rotating deformable wheel is similar to the expressions for rigid wheel, but the modified wheel radius of the deformed shape is considered instead of a constant wheel radius.

$$\sigma(\theta) = \begin{cases} (r(\theta))^n \left(\frac{k_c}{b} + k_{phi}\right) [cos\theta - cos\theta_f]^n & : \theta_m \leq \theta < \theta_f \\ (r(\theta))^n \left(\frac{k_c}{b} + k_{phi}\right) \left[cos\left(\theta_f - \frac{\theta - \theta_r}{\theta_m - \theta_r}(\theta_f - \theta_m)\right) - cos\theta_f\right]^n & : \theta_r < \theta \leq \theta_m \end{cases} \tag{4.19}$$

$$\tau(\theta) = (c + \sigma(\theta)tan\phi)\left[1 - e^{\frac{r(\theta)}{k}\left[\theta_f - \theta - (1-s)(sin\theta_f - sin\theta)\right]}\right] \tag{4.20}$$

Resultant Forces and Torque

The normal and shear stress distributions below the wheel can be converted into resultant forces and torque acting at the wheel center. The net force in x-direction is called as the 'Drawbar Pull'. The expression for drawbar pull is obtained from the $\sigma(\theta)$ and $\tau(\theta)$ expressions:

$$F_x = b \int_{\theta_r}^{\theta_f} r(\theta) \left[\tau(\theta) cos\theta - \sigma(\theta) sin\theta\right] d\theta \tag{4.21}$$

The net-force in y-direction is called as the 'Vertical Force' and is obtained in the same way as Eq.4.21

$$F_y = b \int_{\theta_r}^{\theta_f} r(\theta) \left[\tau(\theta) sin\theta + \sigma(\theta) cos\theta\right] d\theta \tag{4.22}$$

The shear stress distribution results in a net torque about the axis of rotation of the wheel passing through the wheel center. The expression for this torque is derived as:

$$T = b \int_{\theta_r}^{\theta_f} (r(\theta))^2 \tau(\theta) d\theta \tag{4.23}$$

4.3 Drive motor characteristics

4.3.1 Working Principle of DC motors

Direct Current (DC) motors are the most preferred choice for drive motors of mobility system for mars rover prototypes owing to their simpler control and operation on a constant voltage battery. There are different kinds of DC motors like permanent magnet DC motor, brushless DC motors etc. The characteristics can vary from type to type, but the basic principle for DC motors remains the same. "When a permanent magnet is positioned around a loop of wire that is hooked up to a D.C. power source, we have the basics of a D.C. motor (shown in Fig4.6). In order to make the loop of wire spin, we have to connect a battery or DC power supply between its ends, and support it so it can spin about its axis. To allow the rotor to turn without twisting the wires, the ends of the wire loop are connected to a set of contacts called the commutator, which rubs against a set of conductors called the brushes. The brushes make electrical contact with the commutator as it spins, and are connected to the positive and negative leads of the power source, allowing electricity to flow through the loop. The electricity flowing through the loop creates a magnetic field that interacts with the magnetic field of the permanent magnet to make the loop spin" [7]

4.3.2 DC motor characteristics

The Fig.4.7 shows the typical torque vs rotational speed curve for a DC motor. In this graph, τ_s represents the maximum torque that can be supplied by the motor which corresponds to zero rotational speed or stall condition and ω_n represents the maximum speed of the motor which corresponds to zero torque or no load condition.

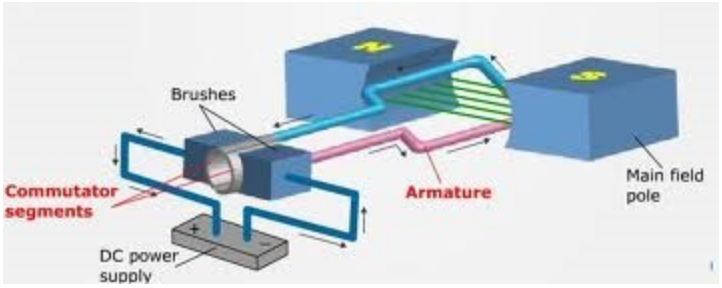

Figure 4.6: DC motor working principle [Courtesy: UStudy]

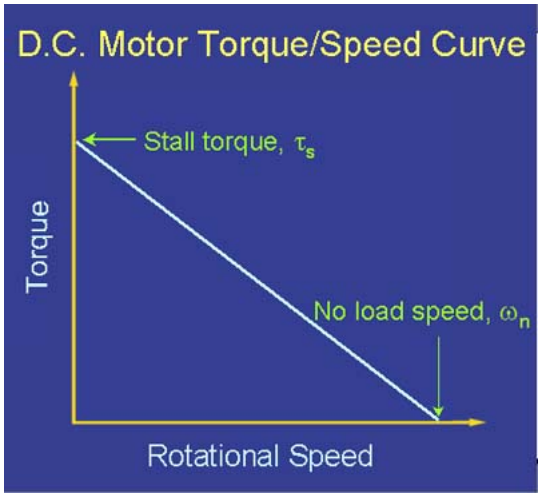

Figure 4.7: DC motor characteristics [7]

The motor characteristics can be altered by changing the voltage applied across the two terminals of motor. In digital circuits, this is achieved by using the concept of Pulse-Width-Modulation (PWM). PWM uses a rectangular pulse wave for input voltage whose pulse is modulated resulting in the variation of the average value of the input voltage. 'Duty cycle' of PWM is defined as the ratio of ON-time and total time period of the square wave. Fig.4.8 shows the variation of input voltage waveform for different duty cycles. PWM allows finer control of the DC motor and reduces the loss due to heat.

The input power of DC motor is calculated as:

$$P = \tau * \omega \tag{4.24}$$

If the input current (I) is not restricted, then the value of Stall Torque τ_s for a DC motor remains independent of the PWM duty cycle. However, the no-load rotational speed ω_n decreases linearly with decrease in PWM duty cycle:

$$\omega_n' = \omega_n * \frac{\delta}{100} \tag{4.25}$$

where δ is the PWM duty cycle (%) and ω_n' is the no-load RPM for given PWM duty cycle.

Thus the modified motor characteristics are shown in Fig.4.9. For a given RPM the

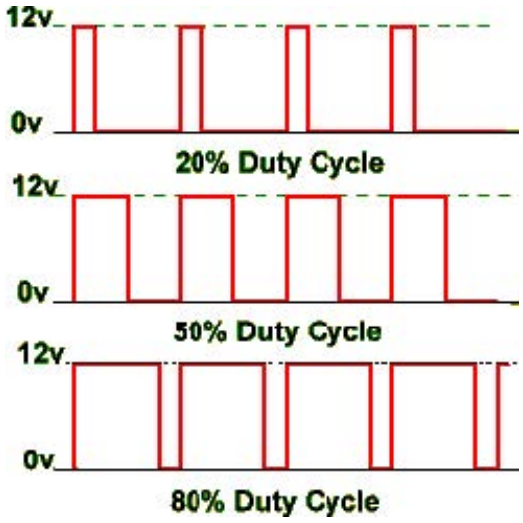

Figure 4.8: Pulse Width Modulation Duty Cycle

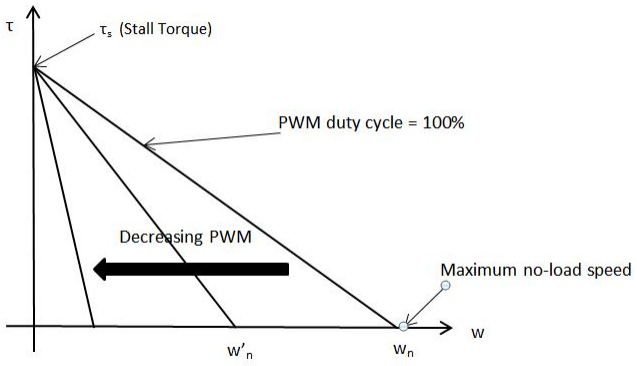

Figure 4.9: Effect of PWM duty cycle on motor characteristics

motor torque is given by:

$$\tau = \tau_s - \frac{\omega * \tau_s}{\omega'_n} \tag{4.26}$$

Substituting the expression for ω'_n, we get the relation between PWM duty cycle and motor torque:

$$\tau = \tau_s - \frac{\omega * \tau_s}{\omega_n} * \frac{100}{\delta} \tag{4.27}$$

In this equation, τ_s and ω_n are constant for a given DC motor. So we can obtain the value of output torque for a given RPM of the motor. The output power of DC motor is evaluated by substituting the values of output torque and rotational speed in Eq.4.24. The input power is given by:

$$P_{input} = V * I \tag{4.28}$$

where V is related to the applied PWM duty cycle and maximum operating voltage of the

motor by:

$$V = \frac{\delta}{100} * V_{operating} \tag{4.29}$$

and I is related to the maximum current or stall current I_s, stall torque and applied torque of the motor:

$$I = \frac{\tau * I_s}{\tau_s} \tag{4.30}$$

Thus input power can be calculated for given PWM duty cycle and applied torque of the motor using Eq.4.28, 4.29 and 4.30

4.4 Rocker Bogie Modeling

4.4.1 3D Kinematic Parameters

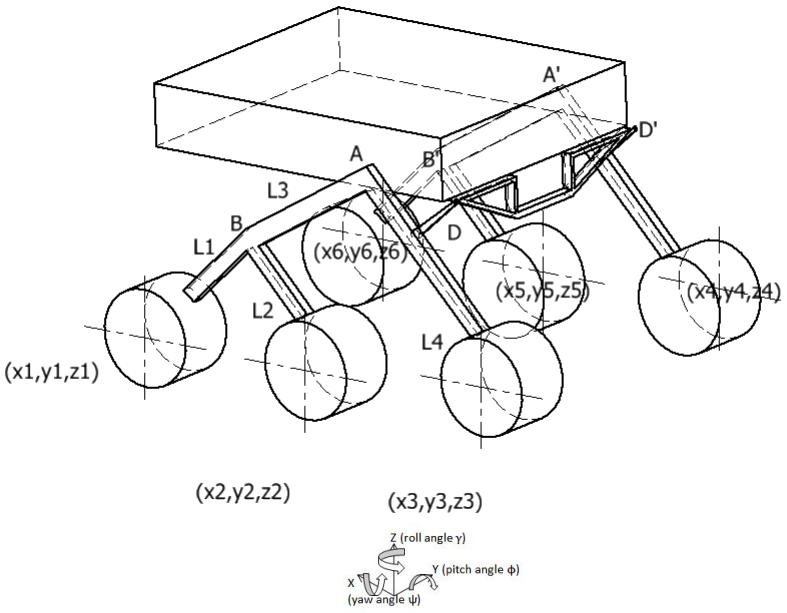

Figure 4.10: 3D Kinematic parameters of rocker bogie

As shown in the above figure, (x_i, y_i, z_i) are the co-ordinates of wheel centers in ground frame, with axes as shown. The origin can be taken at the point of intersection of vertical tangent to the rear wheel and flat ground. L_1, L_2, L_3, L_4 are the lengths of rocker bogie links, Points A and A' represent the rocker-chassis pin joints, Points B and B' represent the rocker-bogie pin joints, Points D and D' represent the differential-rocker pin joints.

4.4.2 Simplified System Model and Design Parameters

Two sides of the rover are identical in the rocker-bogie suspension system. However the displacements and forces at the corresponding joints on either side can be different if the

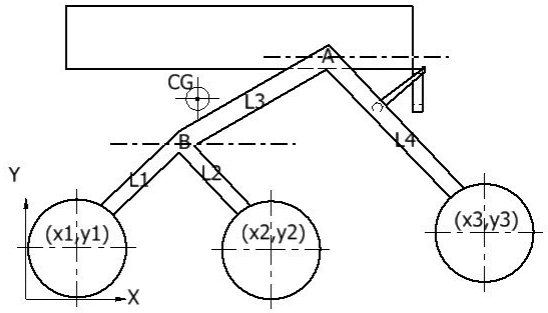

Figure 4.11: 2D model of rocker bogie system

terrain profile is different on either side of the rover. Furthermore the pitch and roll motions of the chassis are coupled with each other when the rover is moving on uneven terrain.

For simplified calculations, this work focuses on design optimization and motion dynamics of single side of the rocker bogie suspension. The analysis is valid for cases where the ground profile on either side of the rover is identical. Thus we neglect the roll and yaw motions of the chassis. Even though this assumption may not be true in natural terrain, it allows us to analyse the effect of change in design parameters on rover's performance metrics, which is the motivation behind developing this simulation tool. The simplified model of single side of rocker-bogie is shown in Fig.4.11

4.4.3 Kinematic Modeling

The attitude and configuration of a rover as a function of terrain on which it moves is required to calculate the load distribution on the wheels, the rover's stability, actuator outputs etc. The positions of wheels on ground are taken as input, the configuration of rocker bogie is evaluated using the procedure described below.

The position of point B can be computed in terms of wheel center co-ordinates and link lengths from following relations:

$$(x_B - x_1)^2 + (y_B - y_1)^2 = L_1^2 \tag{4.31}$$

$$(x_B - x_2)^2 + (y_B - y_2)^2 = L_2^2 \tag{4.32}$$

Once the location of point B is obtained, A can also be obtained in similar way:

$$(x_A - x_3)^2 + (y_A - y_3)^2 = L_4^2 \tag{4.33}$$

$$(x_A - x_B)^2 + (y_A - y_B)^2 = L_3^2 \tag{4.34}$$

The angles of rocker and bogie with respect to the x-axis are given by:

$$\theta_{rocker} = tan^{-1}\left(\frac{y_A - y_3}{x_A - x_3}\right) \tag{4.35}$$

$$\theta_{bogie} = tan^{-1}\left(\frac{y_B - y_2}{x_B - x_2}\right) \tag{4.36}$$

Since the rockers are connected to the main body with a mechanical differential, the pitch angle of the body is the average of pitch angles of the rockers. However in our case, since the ground profile on either side of the rover is assumed to be the same, pitch angle of chassis is given by:

$$\Theta = Pitch\ angle\ of\ chassis = \theta_{rocker} - \theta_{rocker\ initial} \tag{4.37}$$

where $\theta_{rocker\ initial}$ is the rocker angle when the pitch of chassis is 0 i.e. when the rover is standing on flat ground.

Thus we've obtained the chassis attitude and rocker-bogie configuration in terms of wheel center co-ordinates and link lengths.

4.4.4 Motion Dynamics

During the motion of rover, the only external forces acting on it are the forces on wheels due to wheel-terrain interaction and the force due to gravitational pull. The wheel-terrain interaction model was developed in Section 4.3. It was shown that the resultant of wheel-terrain interaction forces is given by force components in each of the x and y directions along with a moment about z-direction (out of plane in our case) acting at the wheel center. Fig.4.12 shows the free body diagram (FBD) of the rover for any given configuration.

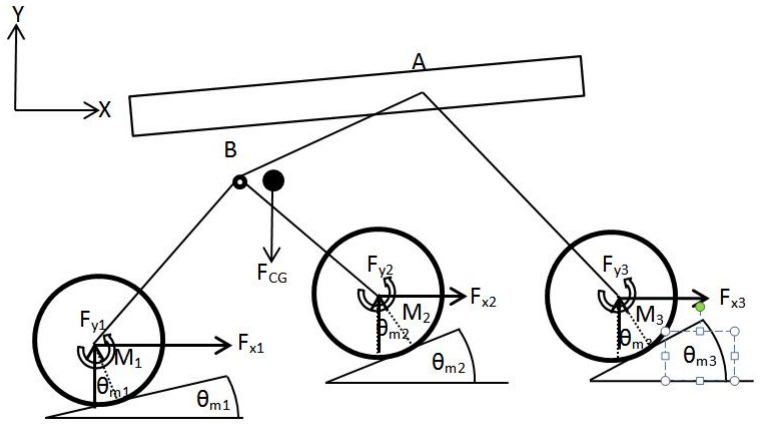

Figure 4.12: Force Analysis

Here F_{xi} and F_{yi} are the forces in x and y direction respectively, M_i are the moments about z-direction (out of plane), θ_{mi} are the mean contact angles.

Since the rocker is connected to the bogie through a pin joint at point B, no axial torque is transmitted through the pivot B. We can consider the system to be made up of two rigid bodies: Rocker+Chassis and Bogie, connected to each other through a pin joint as shown in Fig.4.13 and Fig.4.14

The motion of any rigid body can be defined as the combination of linear motion of it's center of mass and rotation of the body about it's center of mass. Thus forward dynamics equations are derived for both these rigid bodies, by considering the accelerations of center of mass and angular acceleration about center of mass as the unknown parameters.

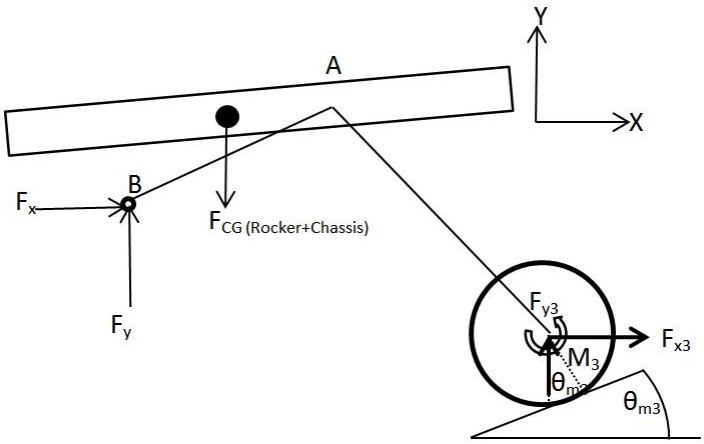

Figure 4.13: Rigid Body 1: Rocker+Chassis

Equations for rocker+chassis:

$$w_{rc} * ax_{rc} = F_x + F_{x3} \tag{4.38}$$

$$w_{rc} * ay_{rc} = F_y + F_{y3} - w_{rc} * g \tag{4.39}$$

$$I_{rc} * \alpha_{rc} = M_3 + F_{y3} * (x_3 - x_{cg\_rc}) + F_{x3} * (y_{cg\_rc} - y_3) + F_x * (y_{cg\_rc} - y_b) + F_y * (x_b - x_{cg\_rc}) \tag{4.40}$$

where w_{rc} - Weight of rocker and chassis
ax_{rc}, ay_{rc} - Acceleration of center of mass of rocker and chassis in x-direction and y-directions
I_{rc} - Moment of Inertia of rocker and chassis about its center of mass
α_{rc} - Angular acceleration of rocker and chassis about its center of mass.

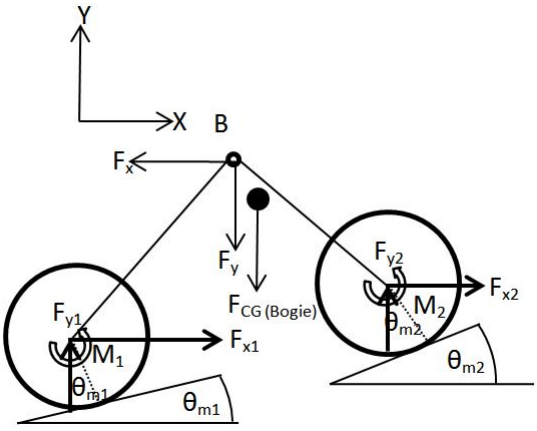

Figure 4.14: Rigid Body 2: Bogie

Equations for bogie:

$$w_{bogie} * ax_{bogie} = -F_x + F_{x1} + F_{x2} \tag{4.41}$$

$$w_{bogie} * ay_{bogie} = -F_y + F_{y1} + F_{y2} - w_{bogie} * g \tag{4.42}$$

$$\begin{aligned} I_{bogie} * \alpha_{bogie} = M_1 + F_{y1} * (x_1 - x_{cg\_bogie}) + F_{x1} * (y_{cg\_bogie} - y_1) \\ M_2 + F_{y2} * (x_2 - x_{cg\_bogie}) + F_{x2} * (y_{cg\_bogie} - y_2) \\ -F_x * (y_{cg\_bogie} - y_b) - F_y * (x_b - x_{cg\_bogie}) \end{aligned} \tag{4.43}$$

where w_{bogie} - Weight of bogie
ax_{bogie}, ay_{bogie} - Acceleration of center of mass of bogie in x-direction and y-directions
I_{bogie} - Moment of Inertia of bogie about its center of mass
α_{bogie} - Angular acceleration of bogie about its center of mass.

Now the velocity components of any point in bogie along x and y directions can be given in terms of the velocity of its center of mass and the angular velocity about its center of mass:

$$v_x = v_{x\_cgbogie} + \omega_{bogie} * (y_{cg\_bogie} - y) \tag{4.44}$$

$$v_y = v_{y\_cgbogie} - \omega_{bogie} * (x_{cg\_bogie} - x) \tag{4.45}$$

where x, y - Position of any arbitrary point in bogie
v_x, v_y - Velocity of that arbitrary point in bogie
$x_{cg\_bogie}, y_{cg\_bogie}$ - Position of center of mass of bogie
$v_{x\_cgbogie}, v_{y\_cgbogie}$ - Velocity of center of mass of bogie
ω_{bogie} - Angular velocity of bogie about its center of mass

Differentiating above equations with respect to time we obtain the relation between acceleration of any point in bogie as:

$$a_x = a_{x\_cgbogie} + \alpha_{bogie} * (y_{cg\_bogie} - y) + \omega_{bogie} * (v_{y\_cgbogie} - v_y) \tag{4.46}$$

$$a_y = a_{y\_cgbogie} - \alpha_{bogie} * (x_{cg\_bogie} - x) - \omega_{bogie} * (v_{x\_cgbogie} - v_x) \tag{4.47}$$

Similar equations can be derived for acceleration of any point in rocker-chassis rigid body,

$$a_x = a_{x\_cgrc} + \alpha_{rc} * (y_{cg\_rc} - y) + \omega_{rc} * (v_{y\_cgrc} - v_y) \tag{4.48}$$

$$a_y = a_{y\_cgrc} - \alpha_{rc} * (x_{cg\_rc} - x) - \omega_{rc} * (v_{x\_cgrc} - v_x) \tag{4.49}$$

Since the point B is common to both the bodies, we obtain following equations by equating Eq.4.46 with Eq.4.48 and Eq.4.47 with Eq.4.49 for $x = x_b$ and $y = y_b$

$$\begin{aligned} a_{x\_cgbogie} + \alpha_{bogie} * (y_{cg\_bogie} - y_b) + \omega_{bogie} * (v_{y\_cgbogie} - v_{y\_b}) \\ = a_{x\_cgrc} + \alpha_{rc} * (y_{cg\_rc} - y_b) + \omega_{rc} * (v_{y\_cgrc} - v_{y\_b}) \end{aligned} \tag{4.50}$$

$$\begin{aligned} a_{y\_cgbogie} - \alpha_{bogie} * (x_{cg\_bogie} - x_b) - \omega_{bogie} * (v_{x\_cgbogie} - v_{x\_b}) \\ = a_{y\_cgrc} - \alpha_{rc} * (x_{cg\_rc} - x_b) - \omega_{rc} * (v_{y\_cgrc} - v_{y\_b}) \end{aligned} \tag{4.51}$$

So we now have 8 linear equations: Eq.4.38 to Eq.4.43, Eq.4.50 and Eq.4.51 in 8 unknowns viz. $F_x, F_y, \alpha_{rc}, \alpha_{bogie}, ax_{rc}, ay_{rc}, ax_{bogie}, ay_{bogie}$ The solution of this system of equations is substituted in Eq.4.46 to Eq.4.49 to get the accelerations of wheel centers, bogie pivot point B and rocker-chassis pivot point A.

During the motion of rover, one or more wheels can lose contact with ground. This scenario has also been taken care of in the simulation model by substituting the wheel sinkage and resultant forces on corresponding wheels as zero in the dynamics equations.

4.4.5 Static Load Distribution

For calculating the initial sinkages of wheels, we need to obtain the initial load on each wheel when the rover is at rest. The static equilibrium equations are obtained by neglecting the acceleration, drawbar pull and resultant moment in Eq.4.38 to Eq.4.43:

$$F_x = 0 \tag{4.52}$$

$$F_y + F_{y3} - w_{rc} * g = 0 \tag{4.53}$$

$$F_{y3} * (x_3 - x_{cg\_rc}) + F_y * (x_b - x_{cg\_rc}) = 0 \tag{4.54}$$

$$F_x = 0 \tag{4.55}$$

$$-F_y - w_{bogie} * g = 0 \tag{4.56}$$

$$-F_{y1} * (x_1 - x_{cg\_bogie}) - F_{y2} * (x_2 - x_{cg\_bogie}) + F_y * (x_b - x_{cg\_bogie}) = 0 \tag{4.57}$$

By solving this system of linear equations we can obtain the vertical load on each wheel i.e. F_{y1}, F_{y2}, F_{y3} in terms of the design parameters and weight data.

4.5 Forward Dynamics Simulation

4.5.1 Computational Flow

The dynamic motion simulation model for the rocker bogie suspension system developed in this thesis is implemented in MATLAB for numerical computations. Currently the contact model for deformable wheel travelling over deformable terrain proposed in Section 4.2.2 is not implemented in the motion dynamics simulation tool due to computational limitations and lack of physical validation owing to time constraints on this thesis work. Fig.4.15 shows the computational flow of the motion dynamics simulation tool.

4.5.2 Sample Simulation Results

The motion dynamics simulation tool is tested using some terrain profiles and design parameters. Three types of terrain profiles are considered:

1. Horizontal flat ground
2. Straight incline of 20degrees
3. Obstacle modelled by a sinusoidal profile

Table 4.1 lists the input parameters given in the motion simulation.

Terrain Profile 1: Flat Ground

As shown in Fig.4.17, the motion of wheel centers and pivot points of rocker-bogie system is in conformance with the ground profile. In this scenario, initially the rover is kept at rest and sudden torque is applied by the drive motors in the beginning. This results in initial slippage as depicted in Fig.4.18. The slip ratio converges to a near zero value in steady state. If the rover rover is initially said to be moving at a constant velocity, the slip ratio remains at a near zero value, as shown in Fig.4.19.

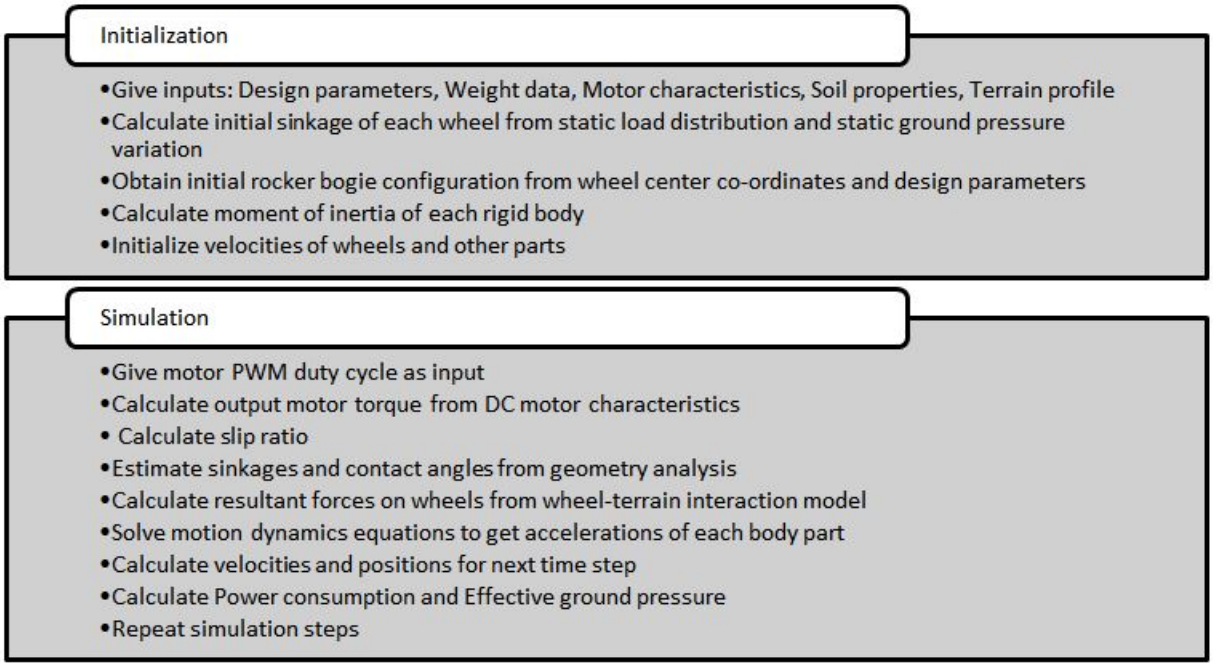

Figure 4.15: Computational Flow of Motion Dynamics Simulation Tool

Terrain Profile 2: Incline of 20degrees

The motion of front wheel over incline of 20 degrees is depicted in Fig.4.20. In this scenario, initially the rover is assumed to travel with a constant velocity. Thus the slip ratio is initially zero, but as the front wheel starts climbing over the slope, its slip ratio increases to a magnitude of 0.2.

Terrain Profile 3: Sinusoidal obstacle

The motion of rover over an obstacle of height 15cm modelled using sinusoidal ground profile is depicted in Fig.4.22. In this scenario, initially the rover is assumed to travel with a constant velocity. Thus the slip ratio is initially zero, but as the front wheel starts climbing over the slope, the magnitude of its slip ratio (s3) increases to 0.2. Later when the middle wheel starts climbing the obstacle, the slip ratios of both middle and rear wheels increase to a magnitude of about 0.2, while the slip ratio of front wheel increases further to a magnitude of about 0.3.

Table 4.1: Input parameters

1) Design variables: r = Radius of wheels = 0.15m, b = Width of wheels = 0.2m, x1 = x2 = Wheel base = 0.45m, (xb,yb) = Position of bogie pivot = (0.375m,0.45m), (xa, ya) = Position of rocker pivot = (0.5m,0.5m)	2) Weight data: Weight of wheel = 2kg, Weight of motor = 2kg, Weight of chassis = 30kg, Total weight of rover = 57.42kg
3) Motor Characteristics: Voltage = 24V, Stall Torque = 30N.m, PWM duty cycle = 50 Maximum no-load speed = 50RPM	4) Soil properties: Soil Type - Dry sand, $k_c = 900N.m^{n+1}$, $k_{phi} = 1523400N.m^{n+2}$, $k = 0.025m$, n = 1.1, $c = 1000N/m^2$, $\phi = 30\,\text{deg}$

4.6 Application of Simulation Tool for Autonomous Control of Reconfigurable Wheels

4.6.1 Concept of Reconfigurable Wheels

Experiences with Spirit and Opportunity, the twin Mars Exploration Rovers, showed that one of the major issues that needs to be addressed in order to expand the exploration capabilities of planetary rovers is that of wheel traction. The relationships governing how much traction a wheel can produce are highly dependent on both the shape of the wheel and terrain properties. In the past, it has always been a challenge to find the right balance between designing a rover wheel with high traction capabilities and low power requirements. More recently, researchers invented the idea of a reconfigurable wheel which would have the ability to change its shape to adapt to the type of terrain it was on[8]. In challenging terrain environments, the wheel could configure to a size that would maximize traction. In less challenging terrain environments, the wheel could configure to a size that would minimize power.

Various mechanisms have been proposed for shape changing or re-configurable wheels. Fig.4.16 shows the re-configurable wheel prototype developed at Massachussets Institute of Technology. In this prototype, the wheel consists of spring steel strips and wire mesh. The strips are attached to two hubcaps connected by a linear actuator. Thus when the linear actuator moves, the strips buckle and there is a change in wheel dimensions. Increase in wheel radius is accompanied by decrease in wheel width, whereas decrease in wheel radius is accompanied by increase in wheel width.

Figure 4.16: Reconfigurable wheel prototype developed at MIT [8]

4.6.2 Autonomous Control of Reconfigurable Wheels

One of the major challenges in implementation of re-configurable wheel is autonomy and control. The wheel should be able to autonomously change its shape based on the terrain characteristics on which it is moving. Some researchers have developed methods for online terrain characterization of the rover[9]. Using these techniques we can estimate the soil characteristics of the terrain on which the rover is moving. To estimate the terrain profile, vision based techniques have been proposed [23].

The terrain characteristics can be given as input to the dynamic simulation model developed in this thesis. By simulating the performance of rover for different wheel dimensions, we can get the optimum values of wheel dimensions for given terrain. The results of simulation can be converted into look-up tables and fed into the on-board rover software. Thus whenever a particular type of terrain is encountered the on-board controller will be able to devise the optimum wheel dimensions using these look up tables. The advantage of this method is that, the onboard computation is very less. However the look up tables have to be made exhaustively for all possible kinds of terrains. This complication can be avoided by developing heuristics based on the simulation results for different kinds of terrains, though this is beyond the scope of this thesis.

For testing the effectiveness of this approach, some test scenarios are considered in this section. The terrain characteristics for these scenarios are given in Table 4.2, while the soil properties for different soil types are given in Table 4.3. The wheel dimensions considered for this exercise are:

1. Set 1: Wheel Diameter = 0.13m, Wheel Width = 0.22m (Minimum radius)
2. Set 2: Wheel Diameter = 0.15m, Wheel Width = 0.20m (Mean radius)
3. Set 3: Wheel Diameter = 0.17m, Wheel Width = 0.18m (Maximum radius)

For all the test scenarios and wheel dimension sets, the performance metrics: Slip Ratio, Power Consumption and Effective Ground Pressure are evaluated and listed in Table 4.4.

For all three performance metrics, a lower value indicates better performance. Thus for each test scenario, a 'Goodness Parameter' is assigned to each wheel configuration. It is

defined as the ratio of difference between the value of performance metric for a given wheel configuration and the lowest value of performance metric amongst the possible wheel configurations to the lowest value of performance metric amongst possible wheel configurations. The weighted sum of goodness parameters for any scenario gives the 'Total Goodness Value' of each wheel configuration for given scenario. Table 4.5 lists the total goodness values of each wheel configuration.

Based on the 'Total Goodness Values' we can develope look-up tables for selecting the best possible wheel configuration in given scenario. Table 4.6 shows the look up table developed for the test scenarios considered in this section. This look up table can be used in on-board rover software to obtain the dimensions of re-configurable wheel for best performance.

Table 4.2: Terrain characteristics for Test scenarios

Test Scenario	Terrain Profile	Soil Type
1	Upward Slope of 20deg	Dry Sand
2	Upward Slope of 20deg	Sandy Loam
3	Upward Slope of 20deg	Clayey Soil
4	Sinusoidal Bump of height 15cm	Dry Sand
5	Sinusoidal Bump of height 15cm	Sandy Loam
6	Sinusoidal Bump of height 15cm	Clayey Soil

Table 4.3: Soil Parameter for Various Soil Types [9]

	Dry Sand	Sandy Loam	Clayey Soil
n	1.1	0.7	0.5
$c(N/m^2)$	1000	1700	4140
ϕ(deg)	30	29	13
$k_c(Pa/m^{n-1})$	900	5300	13200
$k_{phi}(Pa/m^n)$	1523400	1515000	692200
k (m)	0.025	0.025	0.01

Table 4.4: Values of performance metrics for test scenarios

Wheel Configuration	Test Scenario	Slip Ratio	Effective Ground Pressure	Power Consumption
Radius = 0.13m Width = 0.22m	1	0.22	3017	7.988
	2	0.5755	2806	5.256
	3	0.7936	2671	7.27
	4	0.2234	3048	8.64
	5	0.7263	2626	5.844
	6	0.8826	2758	7.814
Radius = 0.15m Width = 0.20m	1	0.1857	3001	9.797
	2	0.5514	2999	7.55
	3	0.7073	2963	8.399
	4	0.1962	2995	9.688
	5	0.629	2898	7.8
	6	0.89	3093	10.15
Radius = 0.17m Width = 0.18m	1	0.157	3096	10.608
	2	0.4541	3076	9.89
	3	0.7025	32816	11.211
	4	0.1329	3138	10.592
	5	0.6066	3017	11.587
	6	0.8588	2956	14.158

Table 4.5: Total Goodness Values for each wheel configuration in different scenarios

Test Scenario	Total Goodness Value		
	Wheel configuration 1	Wheel configuration 2	Wheel configuration 3
1	499	586	664
2	566	543	602
3	635	670	640
4	358	450	673
5	601	638	587
6	686	640	612

Table 4.6: Look Up Table for autonomous reconfiguration of wheel

	Upward Slope	Obstacle
Dry Sand	Wheel Radius = 0.17m, Wheel Width = 0.18m	Wheel Radius = 0.17m, Wheel Width = 0.18m
Sandy Loam	Wheel Radius = 0.17m, Wheel Width = 0.18m	Wheel Radius = 0.15m, Wheel Width = 0.20m
Clayey Soil	Wheel Radius = 0.15m, Wheel Width = 0.20m	Wheel Radius = 0.13m, Wheel Width = 0.22m

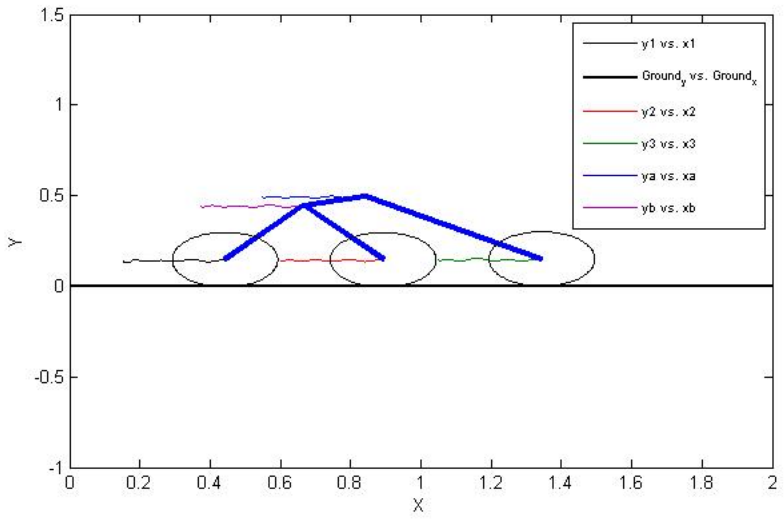

Figure 4.17: Flat Terrain: Plot of Ground Profile and displacements of wheel centers, bogie pivot and rocker pivot

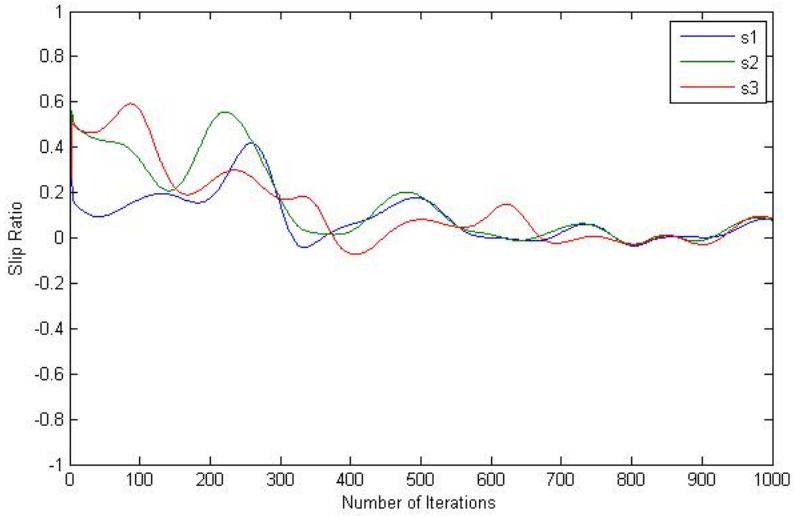

Figure 4.18: Flat Terrain: Plot of Slip Ratio vs Number of Iterations (Initially rover is at rest)

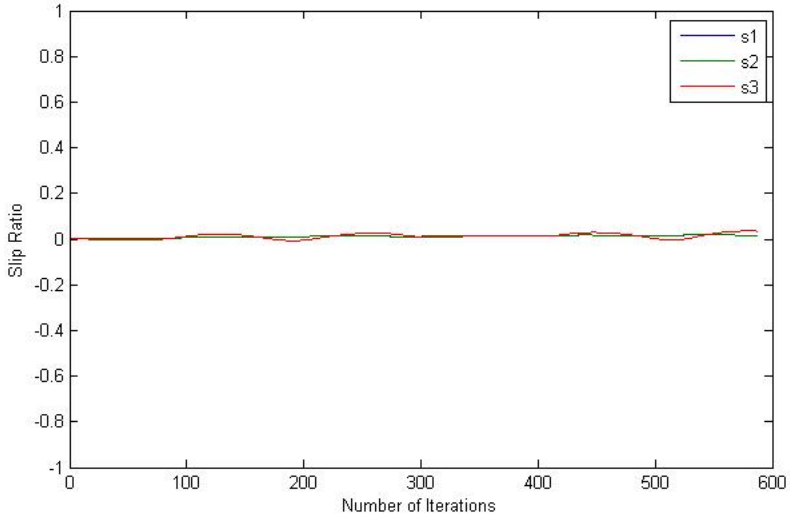

Figure 4.19: Flat Terrain: Plot of Slip Ratio vs Number of Iterations (Initially rover is moving with constant velocity)

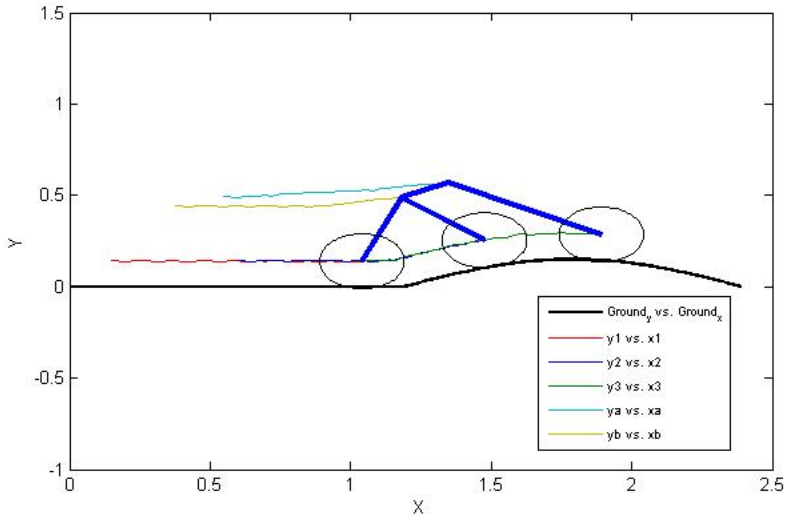

Figure 4.20: Incline: Plot of Ground Profile and displacements of wheel centers, bogie pivot and rocker pivot

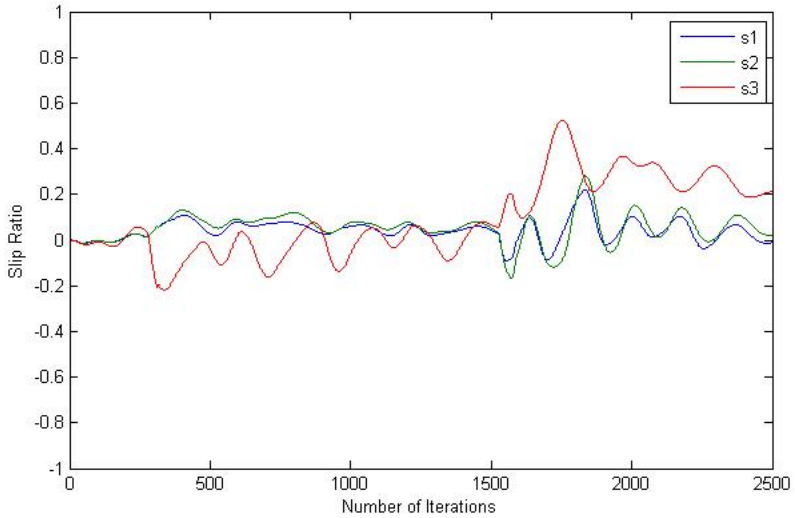

Figure 4.21: Incline: Plot of Slip Ratio vs Number of Iterations

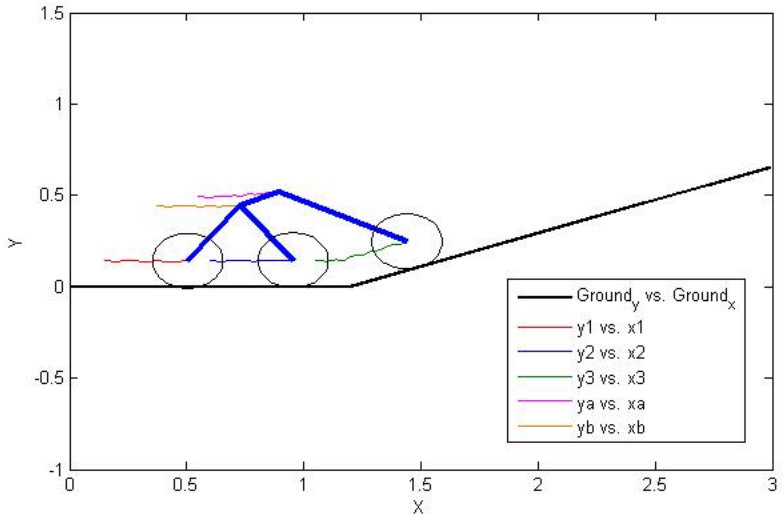

Figure 4.22: Obstacle: Plot of Ground Profile and displacements of wheel centers, bogie pivot and rocker pivot

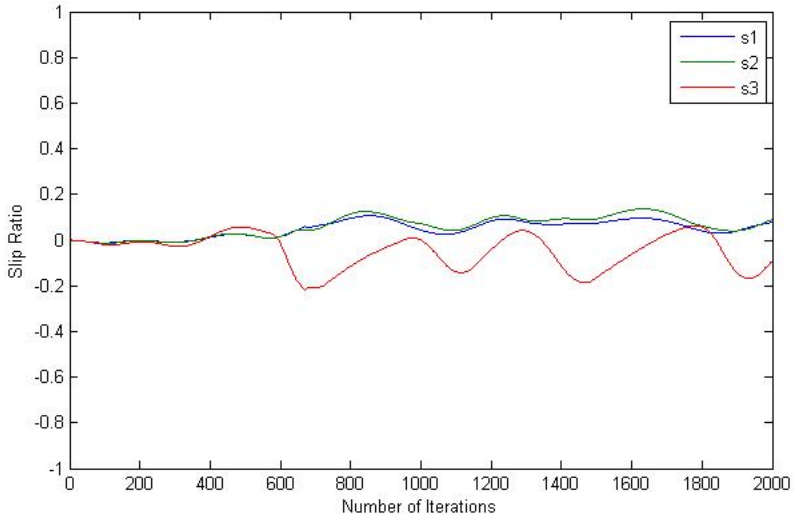

Figure 4.23: Obstacle: Plot of Slip Ratio vs Number of Iterations

Chapter 5

Conclusion and Future Work

5.1 Conclusion

All the objectives of this thesis were successfully met. Various configurations of mobility systems for Planetary Rovers were studied and compared based on certain performance metrics. Amongst the evaluated configurations, six wheel rocker bogie suspension system was found to be most suitable for mars mission. In order to obtain optimum design parameters of rocker bogie suspension system, analytical relations were derived between the design parameters and performance metrics. Through a constrained optimization procedure the optimal design parameters of rocker bogie suspension system were obtained for some mission scenarios. The optimal design parameters were used in development of a mars rover prototype as a research activity of Mars Society India, IIT Bombay.

Next, a terramechanics based motion dynamics model was developed for single side of the rocker-bogie suspension system. Wheel-ground interaction models for rigid and deformable wheels were discussed. A novel technique for calculating the deformed shape of elastic wheel was proposed. A simulation tool was developed in MATLAB, incorporating the rigid wheel over deformable terrain contact model, drive motor characteristics and motion dynamics of rocker bogie suspension system. Sample test cases were presented to validate the simulation tool.

The concept of reconfigurable wheels was discussed with reference to the effect of wheel dimensions on performance metrics of the mobility system for different terrains. The values of three performance metrics viz. Slip Ratio, Power Consumption, Effective Ground Pressure, were obtained using the simulation tool for some test scenarios. Based on the results for different wheel configurations, a look up table was developed for autonomous re-configuration of wheel dimensions.

5.2 Future Work

5.2.1 Design Optimization

During the optimization procedure, it was found that only some of the design parameters were affecting the performance metrics. Thus there is a need to consider more performance

metrics such as overturning stability, lateral stability etc. in the objective function.

5.2.2 Wheel Soil Contact Model

A novel technique for calculating the deformed shape of elastic wheel was proposed in this thesis. However it needs to be physically validated and implemented in the simulation tool.

5.2.3 Motion Dynamics

In this thesis, a simplified model of rocker-bogie suspensions system was considered for developing forward dynamics equations. The roll and yaw degrees of freedom of the chassis were neglected by assuming same ground profile on either side of the rover. In reality, the rover will travel over uneven terrain and the pitch-roll-yaw motions of chassis will be coupled with each other. Thus there is a lot of scope in development and implementation of forward motion dynamics for complete 3D rocker bogie system in the simulation tool.

5.2.4 Applications of Motion Dynamics Simulation Tool

The motion dynamics simulation tool developed in this thesis can be used to test the slip-based traction control strategies for improving the performance of rover on difficult terrain. Also more test cases can be considered for expanding the look up table for autonomous control of reconfigurable wheels. Some heuristics can also be developed by analysing the effect of each soil parameter on performance metrics.

Bibliography

[1] Matthew J. Roman. Design and analysis of a four wheeled planetary rover. Master's thesis, University of Oklahoma, 2005.

[2] Suojun Li, Haibo Gao, and Zongquan Deng. Mobility performance evaluation of lunar rover and optimization of rocker-bogie suspension parameters. *IEEE*, 2008.

[3] Keith Enevoldsen. *http://www.alicesastroinfo.com/2012/07/mars-rover-rocker-bogie-differential/.*

[4] A. Petritsenko and R. Sell. Wheel motion resistance and soil thrust traction of mobile robot. In *8th International DAAAM Baltic Conference*, Tallin, Estonia, 2012.

[5] Genya Ishigami, Masatsugu Otsuki, Takashi Kubota, and Karl Iagnemma. Modeling of flexible and rigid wheels for exploration rover on rough terrain. In *28th International Symposium on Space Technology and Science*, Okinawa, Japan, 2011.

[6] Genya Ishigami, Akiko Miwa, Keiji Nagatani, and Kazuya Yoshida. Terramechanics-based model for steering maneuver of planetary exploration rovers on loose soil. *Journal of Field Robotics*, 2007.

[7] Masachussets Institute of Technology Center for Innocation in Product Development. *http://lancet.mit.edu/motors/motors3.html.*

[8] Brittany Bekker. Re-inventing the wheel for the next generation of planetary rovers. Master's thesis, Massachusetts Institute of Technology, 2012.

[9] Karl Iagnemma, Shinwoo Kang, Hassan Shibly, and Steven Dubowsky. Online terrain parameter estimation for wheeled mobile robots with application to planetary rovers. *IEEE transactions on Robotics*, 2004.

[10] Garett Sohl and Abhinandan Jain. Wheel-terrain contact modeling in the roams planetary rover simulation. In *ASME International Design Engineering Technical Conferences and Computers and Information in Engineering Conference*, California, USA, 2005.

[11] Resources on NASA/JPL website. *http://www-robotics.jpl.nasa.gov.*

[12] Brian D. Harrington and Chris Voorhees. The challenges of designing the rocker-bogie suspension for the mars exploration rover. In *37th Aerospace Mechanisms Symposium*, Johnson Space Center, May 2004.

[13] Thomas Thuer. *Mobility evaluation of wheeled all-terrain robots: Metrics and application*. PhD thesis, ETH Zurich, 2009.

[14] Randy Lindemann. Broader interests and applica1ons the view of a jpl hardware engineer. Technical report, Jet Propulsion Laboratory, California Institute of Technology, 2011.

[15] D.Lachat. Antarctica rover design and optimization for limited power consumption. EPFL, Switzerland.

[16] J.Y. Wong. *Theory of Ground Vehicles*. Wiley, New York, 2008.

[17] Christopher Brunskill, Nildeep Patel, Thibault P. Gouachea, Gregory P. Scott, Chakravarthini M. Saaj, Marcus Matthews, and Liang Cui. Characterisation of martian soil simulants for the exomars rover testbed. *Journal of Terramechanics*, 2011.

[18] M. Bekker. *Off-The-Road Locomotion*. The University of Michigan, 1960.

[19] Kazuya Yoshida and Hiroshi Hamano. Motion dynamics of a rover with slip-based traction model. In *IEEE International Conference on Robotics and Automation*, Washington, DC, USA, 2002.

[20] K. Yoshida et. al. erramechanics-based analysis and traction control of a lunar/planetary rover. In *International Conference on Field and Service Robotics*, Yamanashi, Japan, 2003.

[21] J. Y. Wong and A. Reece. Prediction of rigid wheel performance based on the analysis of soil-wheel stresses part i, preformance of driven rigid wheels. *Journal of Terramechanics*, 1967.

[22] Carsten Harnisch et. al. A new tyresoil interaction model for vehicle simulation on deformable ground. *International Journal of Vehicle Mechanics and Mobility*, 2011.

[23] Timothy Barfoot and Piotr Jasiobedzki. Vision-based localization and terrain modeling for planetary rovers. Space Missions, MDA, Canada.

Appendix A

MATLAB source code

The MATLAB simulation tool is developed in the modular form with independent functions for some tasks and a main function.

1. $'simulation1.m'$ is the main program which initialises the parameters and runs the simulation for each timestep.

2. *cg_calculator.m* is the function developed for calculating the positions of center of mass for each rigid body in rocker bogie system.

3. $force\_calculator.m$ is the function developed for calculating wheel-terrain interaction forces.

4. *sinkage_calulator.m* is the function developed for calculating geometric intersections between ground profile and wheel, it uses a function called $intersections.m$ developed by Douglas Schwarz.

```
clear all;
clear;
%% design variables in m
r=0.15;
b=0.20;
l1=0.45;
l2=0.45;
l3=0.45;
l4=0.5;
l5=0.375;
l6=0.55;
g = 3.711; %gravity on mars m/s^2
l7 = 0.6; %CG of chassis
l8 = 0.5;
l9 = 0.5; %radius of gyration of chassis

%% link lengths
r1 = sqrt((l5-r)^2+(l3-r)^2);
r2 = sqrt((l5-r-l1)^2+(l3-r)^2);
r3 = sqrt((l5-l6)^2+(l3-l4)^2);
r4 = sqrt((r+l1+l2-l6)^2+(r-l4)^2);
rchassis = sqrt((l7-l6)^2+(l8-l4)^2);%distance between rocker hinge and chassis CG
r5 = sqrt((r+l1+l2-l5)^2+(l3-r)^2); %imaginary link between rocker wheel and b

%% Weight data
wheel = 2; %kg
motor = 2; %kg
w_chassis = 30; %kg
w_m = wheel +motor;
rho = 10; %kg/m linear density of links
w_r1 = rho*r1;
w_r2 = rho*r2;
w_r3 = rho*r3;
w_r4 = rho*r4;

w_rocker = w_m + w_r3 + w_r4;
w_bogie = w_m + w_m + w_r1 + w_r2;
w_rc = w_rocker + w_chassis;
w_total = w_bogie + w_rocker + w_chassis;

%% motor characteristics
voltage = 24; %V
stall_torque = 30; %N.m
wn_max = 50*2*pi/60;
stall_current = 10; %amps


%% soil properties (turning force calculations and wheel-soil interaction)
%Dry Sand
kc = 900; %N.m^(n+1)
kphi = 1523400; %N.m^(n+2)
k = 0.025; %m
n = 1.1;
c=1000;
phi = 30*pi/180;
```

```
% %Sandy loam
% kc = 5300; %N.m^(n+1)
% kphi = 1515000; %N.m^(n+2)
% k = 0.025; %m
% n = 0.7;
% c=1700;
% phi = 29*pi/180;

% % Clayey Soil
% kc = 13200; %N.m^(n+1)
% kphi = 692200; %N.m^(n+2)
% k = 0.01; %m
% n = 0.5;
% c=4140;
% phi = 13*pi/180;

%% Ground profile
Ground_x = 0:0.01:2.39;
Ground_y = zeros(1,120);
%
for i=121:1:240
Ground_y(i) = tand(20)*(Ground_x(i)-1.2);
% Ground_y(i) = 0.15*sin(pi*(i-120)/120);

end

plot(Ground_x,Ground_y);
drawnow
hold on
%% Static position of wheels
x1(1)=r;
x2(1)=r+l1;
x3(1)=r+l1+l2;
y1(1)=r;
y2(1)=r;
y3(1)=r;

%% Static Rocker bogie configuration
syms x_b y_b x_a y_a;
B =solve((x_b-x1(1))^2+(y_b-y1(1))^2-r1^2,(x_b-x2(1))^2+(y_b-y2(1))^2-r2^2);
if double(B.x_b(1,1))>x1(1)
    xb(1)=double(B.x_b(1,1));
else
    xb(1)=double(B.x_b(2,1));
end
if double(B.y_b(1,1))>y1(1)
    yb(1)=double(B.y_b(1,1));
else
    yb(1)= double(B.y_b(2,1));
end

A = solve((x_a-x3)^2+(y_a-y3)^2-r4^2,(x_a-xb(1))^2+(y_a-yb(1))^2-r3^2);
if double(A.x_a(1,1))>xb(1)
```

```
    xa(1)=double(A.x_a(1,1));
else
    xa(1)=double(A.x_a(2,1));
end
if double(A.y_a(1,1))>yb(1)
    ya(1)=double(A.y_a(1,1));
else
    ya(1)= double(A.y_a(2,1));
end

alpha1_initial = atan((ya(1)-y3(1))/(x3(1)-xa(1))); %rocker angle
alpha2_initial = atan((yb(1)-y2(1))/(x3(1)-xb(1))); %bogie angle
alpha3 = atan((l8-ya(1))/(l7-xa(1))); %chassis CG angle
pitch(1) = alpha1_initial - atan((ya(1)-y3(1))/(x3(1)-xa(1))) ;

[ x_cg_bogie(1), y_cg_bogie(1), x_cg_rocker(1), y_cg_rocker(1), x_cg_chassis(1),↙
y_cg_chassis(1), x_cg_rc(1), y_cg_rc(1), x_cg(1), y_cg(1) ] = cg_calculator( x1(1),y1↙
(1),x2(1),y2(1),x3(1),y3(1),xa(1),ya(1),xb(1),yb(1),rchassis,alpha3,pitch(1),w_m,w_r1,↙
w_r2,w_r3,w_r4,w_rocker,w_bogie,w_chassis,w_total);

%% Calculate initial sinkage
syms F_y F_n1 F_n2 F_n3;
eq1 = F_y  - F_n1 - F_n2  + w_bogie*g ;

eq2 = - F_n1 *(x1(1) - x_cg_bogie(1)) - F_n2 *(x2(1) - x_cg_bogie(1))-F_y*(x_cg_bogie↙
(1)-xb(1));

eq3 = -F_y - F_n3 + w_rc*g;

eq4 = - F_n3 *(x3(1) - x_cg_rc(1))+F_y*(x_cg_rc(1)-xb(1));

I = solve(eq1,eq2,eq3,eq4);
F_y = double(I.F_y);
F_n1 = double(I.F_n1);
F_n2 = double(I.F_n2);
F_n3 = double(I.F_n3);
F_n1_initial = F_n1;
F_n2_initial = F_n2;
F_n3_initial = F_n3;


thetas1 = 0.001;
thetas2 = 0.001;
thetas3 = 0.001;
f_z1 = r^(n+1)*(kc+kphi*b)*quad(@(theta)(cos(theta)-cos(thetas1)).^n.*cos(theta),-↙
thetas1,thetas1);
f_z2 = r^(n+1)*(kc+kphi*b)*quad(@(theta)(cos(theta)-cos(thetas2)).^n.*cos(theta),-↙
thetas2,thetas2);
f_z3 = r^(n+1)*(kc+kphi*b)*quad(@(theta)(cos(theta)-cos(thetas3)).^n.*cos(theta),-↙
thetas3,thetas3);
 error1 = abs(f_z1-F_n1_initial);
 error2 = abs(f_z2-F_n2_initial);
 error3 = abs(f_z3-F_n3_initial);

while (error1>0.05*F_n1_initial)
```

```
    thetas1 = thetas1 + 0.001;
    f_z1 = r^(n+1)*(kc+kphi*b)*quad(@(theta)(cos(theta)-cos(thetas1)).^n.*cos(theta),-↙
thetas1,thetas1);
    error1 = abs(f_z1-F_n1_initial)
end
while (error2>0.05*F_n2_initial)
    thetas2 = thetas2 + 0.001;
    f_z2 = r^(n+1)*(kc+kphi*b)*quad(@(theta)(cos(theta)-cos(thetas2)).^n.*cos(theta),-↙
thetas2,thetas2);
    error2 = abs(f_z2-F_n2_initial)
end
while (error3>0.05*F_n3_initial)
    thetas3 = thetas3 + 0.001;
    f_z3 = r^(n+1)*(kc+kphi*b)*quad(@(theta)(cos(theta)-cos(thetas3)).^n.*cos(theta),-↙
thetas3,thetas3);
    error3 = abs(f_z3-F_n3_initial)
end
theta_initial1 = thetas1;
theta_initial2 = thetas2;
theta_initial3 = thetas3;



h_initial1 = r*(1-cos(theta_initial1));
h_initial2 = r*(1-cos(theta_initial2));
h_initial3 = r*(1-cos(theta_initial3));
thetaf1(1) = theta_initial1;
thetaf2(1) = theta_initial2;
thetaf3(1) = theta_initial3;
thetar1(1) = -theta_initial1;
thetar2(1) = -theta_initial2;
thetar3(1) = -theta_initial3;
thetam1(1) = 0;
thetam2(1) = 0;
thetam3(1) = 0;


%% Initial rocker bogie configuration
x1(1)=r;
y1(1)=r-h_initial1;
y2(1)=r-h_initial2;
x2(1)=x1(1) + sqrt(l1^2-(y2(1)-y1(1))^2);



syms x_b y_b x_a y_a;
B =solve((x_b-x1(1))^2+(y_b-y1(1))^2-r1^2,(x_b-x2(1))^2+(y_b-y2(1))^2-r2^2);
if double(B.x_b(1,1))>x1(1)
    xb(1)=double(B.x_b(1,1));
else
    xb(1)=double(B.x_b(2,1));
end
if double(B.y_b(1,1))>y1(1)
    yb(1)=double(B.y_b(1,1));
else
```

```
    yb(1)= double(B.y_b(2,1));
end

y3(1)=r-h_initial3;
x3(1)=xb(1) + sqrt(r5^2-(y3(1)-yb(1))^2);

A = solve((x_a-x3(1))^2+(y_a-y3(1))^2-r4^2,(x_a-xb(1))^2+(y_a-yb(1))^2-r3^2);
if double(A.x_a(1,1))>xb(1)
    xa(1)=double(A.x_a(1,1));
else
    xa(1)=double(A.x_a(2,1));
end
if double(A.y_a(1,1))>yb(1)
    ya(1)=double(A.y_a(1,1));
else
    ya(1)= double(A.y_a(2,1));
end

alpha1(1) = atan((ya(1)-y3(1))/(x3(1)-xa(1))); %rocker angle
alpha2(1) = atan((yb(1)-y2(1))/(x3(1)-xb(1))); %bogie angle
pitch(1) = alpha1_initial - atan((ya(1)-y3(1))/(x3(1)-xa(1))) ;




%% Plot Rocker bogie configuration
axis([-1 5 -1 5])
line([x1 xb],[y1 yb])
line([xb x2],[yb y2])
line([xb xa],[yb ya])
line([xa x3],[ya y3])
rectangle('Position',[x1-r,y1-r,2*r,2*r],'Curvature',[1,1])
rectangle('Position',[x2-r,y2-r,2*r,2*r],'Curvature',[1,1])
rectangle('Position',[x3-r,y3-r,2*r,2*r],'Curvature',[1,1])
%hold on;

%% Simulate
%Initialization
pwm1(1) = 50;
pwm2(1) = 50;
pwm3(1) = 50;

wn1 = wn_max * pwm1(1)/100;
wn2 = wn_max * pwm2(1)/100;
wn3 = wn_max * pwm3(1)/100;

w1(1)= wn_max*pwm1(1)/100;
w2(1)= wn_max*pwm2(1)/100;
w3(1)= wn_max*pwm3(1)/100;
%
% w1(1)= 0;
% w2(1)= 0;
% w3(1)= 0;
```

```
% v1_x(1) = 0;
% v1_y(1) = 0;
% v2_x(1) = 0;
% v2_y(1) = 0;
% v3_x(1) = 0;
% v3_y(1) = 0;
v1_x(1) = w1(1)*r;
v1_y(1) = 0;
v2_x(1) = w1(1)*r;
v2_y(1) = 0;
v3_x(1) = w1(1)*r;
v3_y(1) = 0;
% %
% v_x_rc(1) = 0;
% v_y_rc(1) = 0;
% v_x_b(1) = 0;
% v_y_b(1) = 0;
% v_x_a(1) = 0;
% v_y_a(1) = 0;
% v_x_bogie(1) = 0;
% v_y_bogie(1) = 0;
% omega_rc(1) = 0;
% omega_bogie(1) = 0;
v_x_rc(1) = w1(1)*r;
v_y_rc(1) = 0;
v_x_b(1) = w1(1)*r;
v_y_b(1) = 0;
v_x_a(1) = w1(1)*r;
v_y_a(1) = 0;
v_x_bogie(1) = w1(1)*r;
v_y_bogie(1) = 0;
omega_rc(1) = 0;
omega_bogie(1) = 0;

v1 = sqrt(v1_x(1)^2+v1_y(1)^2);
v2 = sqrt(v2_x(1)^2+v2_y(1)^2);
v3 = sqrt(v3_x(1)^2+v3_y(1)^2);


%% Moment of Inertia calculation
I_bogie = w_m*r1^2+w_m*r2^2+rho*r1^2/3+rho*r2^2/3-w_bogie*((x_cg_bogie(1)-xb(1))^2+↙
(y_cg_bogie(1)-yb(1))^2); %about CG bogie
I_rocker = w_m*r4^2 + rho*r3^2/3+rho*r4^2/3; %about A
I_chassis = w_chassis*(l8)^2 + w_chassis*(l6-l7)^2; %about A
I_rc = I_rocker + I_chassis - w_rc*((x_cg_rc(1)-xa(1))^2+(y_cg_rc(1)-ya(1))^2); %about↙
CG rc


i=1;
delta = 0.001;

%% Simulation
for t=delta:delta:1000*delta

%%Motor Torque Calculation
```

```
torque1(i) = stall_torque - (w1(i)*stall_torque)*100/(wn_max*pwm1(i));
torque2(i) = stall_torque - (w2(i)*stall_torque)*100/(wn_max*pwm2(i));
torque3(i) = stall_torque - (w3(i)*stall_torque)*100/(wn_max*pwm3(i));

%% Slip ratio calculation
if w1 == 0
    s1(i)=0;
else
    if abs(r*w1(i))>v1
    s1(i) = (r*w1(i)-v1)/(r*w1(i));
    else
    s1(i) = (r*w1(i)-v1)/v1;
    end
end

if w2(i) ==0
    s2(i)=0;
else
    if abs(r*w2(i))>v2
    s2(i) = (r*w2(i)-v2)/(r*w2(i));
    else
    s2(i) = (r*w2(i)-v2)/v2;
    end
end

if w3(i) == 0
    s3(i) =0;
else
    if abs(r*w3(i))>v3
    s3(i) = (r*w3(i)-v3)/(r*w3(i));
    else
    s3(i) = (r*w3(i)-v3)/v3;
    end
end


%% Sinkage calculation
[ x_cg_bogie(i), y_cg_bogie(i), x_cg_rocker(i), y_cg_rocker(i), x_cg_chassis(i),↙
y_cg_chassis(i), x_cg_rc(i), y_cg_rc(i), x_cg(i), y_cg(i) ] = cg_calculator( x1(i),y1↙
(i),x2(i),y2(i),x3(i),y3(i),xa(i),ya(i),xb(i),yb(i),rchassis,alpha3,pitch(i),w_m,w_r1,↙
w_r2,w_r3,w_r4,w_rocker,w_bogie,w_chassis,w_total);

m =1;
for thetaw = -pi:pi/100:pi
   Wheel1_x(m) = x1(i)+r*cos(thetaw);
   Wheel1_y(m) = y1(i)-r*sin(thetaw);
   m = m+1;
end
[sinkage1 thetar1(i) thetam1(i) thetaf1(i)]= sinkage_calculator(Ground_x,Ground_y,↙
Wheel1_x,Wheel1_y,x1(i),y1(i),r,s1(i));
m =1;
for thetaw = -pi:pi/100:pi
  Wheel2_x(m) = x2(i)+r*cos(thetaw);
   Wheel2_y(m) = y2(i)-r*sin(thetaw);
   m = m+1;
```

```
end
[sinkage2 thetar2(i) thetam2(i) thetaf2(i)]= sinkage_calculator(Ground_x,Ground_y,↙
Wheel2_x,Wheel2_y,x2(i),y2(i),r,s2(i));

m =1;
for thetaw = -pi:pi/100:pi
  Wheel3_x(m) = x3(i)+r*cos(thetaw);
   Wheel3_y(m) = y3(i)-r*sin(thetaw);
   m = m+1;
end
[sinkage3 thetar3(i) thetam3(i) thetaf3(i)]= sinkage_calculator(Ground_x,Ground_y,↙
Wheel3_x,Wheel3_y,x3(i),y3(i),r,s3(i));


%% Force calculations

[F_n1(i) F_t1(i) M_1(i)] = force_calculator(r,b,thetaf1(i),thetar1(i),thetam1(i),n,kc,↙
kphi,k,c,phi,s1(i));


[F_n2(i) F_t2(i) M_2(i)] = force_calculator(r,b,thetaf2(i),thetar2(i),thetam2(i),n,kc,↙
kphi,k,c,phi,s2(i));


[F_n3(i) F_t3(i) M_3(i)] = force_calculator(r,b,thetaf3(i),thetar3(i),thetam3(i),n,kc,↙
kphi,k,c,phi,s3(i));

%% Motion dynamics



syms ax_bogie_s ay_bogie_s ax_rc_s ay_rc_s alpha_rc_s alpha_bogie_s F_x_s F_y_s;
eqn1 = F_x_s + w_bogie*ax_bogie_s - F_t1(i) - F_t2(i);

eqn2 = F_y_s + w_bogie*ay_bogie_s - F_n1(i) - F_n2(i) + w_bogie*g ;

eqn3 = I_bogie* alpha_bogie_s - M_1(i)-F_t1(i)*(y_cg_bogie(i) - y1(i)) - F_n1(i)*(x1(i)↙
- x_cg_bogie(i)) - M_2(i)-F_t2(i)*(y_cg_bogie(i) - y2(i)) - F_n2(i)*(x2(i) - x_cg_bogie↙
(i))-F_y_s*(x_cg_bogie(i)-xb(i))-F_x_s*(yb(i)-y_cg_bogie(i));

eqn4 = -F_x_s + w_rc*ax_rc_s  - F_t3(i);

eqn5 = -F_y_s + w_rc*ay_rc_s - F_n3(i) + w_rc*g;

eqn6 = I_rc*alpha_rc_s - M_3(i)-F_n3(i)*(x3(i) - x_cg_rc(i)) - F_t3(i)*(y_cg_rc(i) - y3↙
(i))-F_x_s*(y_cg_rc(i)-yb(i))+F_y_s*(x_cg_rc(i)-xb(i));

eqn7 = ax_rc_s + alpha_rc_s*(y_cg_rc(i) - yb(i)) + omega_rc(i)*(v_y_rc(i) - v_y_b(i)) -↙
ax_bogie_s - alpha_bogie_s*(y_cg_bogie(i) - yb(i)) - omega_bogie(i)*(v_y_bogie(i) -↙
v_y_b(i));

eqn8 = ay_rc_s - alpha_rc_s *(x_cg_rc(i) - xb(i)) - omega_rc(i)*(v_x_rc(i) - v_x_b(i))↙
- ay_bogie_s + alpha_bogie_s *(x_cg_bogie(i) - xb(i)) + omega_bogie(i)*(v_x_bogie(i) -↙
v_x_b(i));
```

```
C = solve (-eqn1,-eqn2,-eqn3,-eqn4,-eqn5,-eqn6,-eqn7,-eqn8);
F_x(i) = double(C.F_x_s);
F_y(i) = double(C.F_y_s);
alpha_rc(i) = double(C.alpha_rc_s);
alpha_bogie(i) = double(C.alpha_bogie_s);
ax_rc(i) = double(C.ax_rc_s);
ax_bogie(i) = double(C.ax_bogie_s);
ay_rc(i) = double(C.ay_rc_s);
ay_bogie(i) = double(C.ay_bogie_s);

a1_x(i) = double(ax_bogie(i)+alpha_bogie(i)*(y_cg_bogie(i)-y1(i))+omega_bogie(i)*↙
(v_y_bogie(i)-v1_y(i)));
a1_y(i) = double(ay_bogie(i)-alpha_bogie(i)*(x_cg_bogie(i)-x1(i))-omega_bogie(i)*↙
(v_x_bogie(i)-v1_x(i)));

a2_x(i) = double(ax_bogie(i)+alpha_bogie(i)*(y_cg_bogie(i)-y2(i))+omega_bogie(i)*↙
(v_y_bogie(i)-v2_y(i)));
a2_y(i) = double(ay_bogie(i)-alpha_bogie(i)*(x_cg_bogie(i)-x2(i))-omega_bogie(i)*↙
(v_x_bogie(i)-v2_x(i)));

a3_x(i) = double(ax_rc(i)+alpha_rc(i)*(y_cg_rc(i)-y3(i))+omega_rc(i)*(v_y_rc(i)-v3_y↙
(i)));
a3_y(i) = double(ay_rc(i)-alpha_rc(i)*(x_cg_rc(i)-x3(i))-omega_rc(i)*(v_x_rc(i)-v3_x↙
(i)));

ab_x(i) = double(ax_bogie(i)+alpha_bogie(i)*(y_cg_bogie(i)-yb(i))+omega_bogie(i)*↙
(v_y_bogie(i)-v_y_b(i)));
ab_y(i) = double(ay_bogie(i)-alpha_bogie(i)*(x_cg_bogie(i)-xb(i))-omega_bogie(i)*↙
(v_x_bogie(i)-v_x_b(i)));

aa_x(i) = double(ax_rc(i)+alpha_rc(i)*(y_cg_rc(i)-ya(i))+omega_rc(i)*(v_y_rc(i)-v_y_a↙
(i)));
aa_y(i) = double(ay_rc(i)-alpha_rc(i)*(x_cg_rc(i)-xa(i))-omega_bogie(i)*(v_x_rc(i)-↙
v_x_a(i)));

%% Next timestep velocity calculation
v1_x(i+1) = v1_x(i)+a1_x(i)*delta;
v1_y(i+1) = v1_y(i)+a1_y(i)*delta;
v2_x(i+1) = v2_x(i)+a2_x(i)*delta;
v2_y(i+1) = v2_y(i)+a2_y(i)*delta;
v3_x(i+1) = v3_x(i)+a3_x(i)*delta;
v3_y(i+1) = v3_y(i)+a3_y(i)*delta;
v1 = sqrt(v1_x(i+1)^2+v1_y(i+1)^2);
v2 = sqrt(v2_x(i+1)^2+v2_y(i+1)^2);
v3 = sqrt(v3_x(i+1)^2+v3_y(i+1)^2);

v_x_bogie(i+1) = v_x_bogie(i) + ax_bogie(i)*delta;
v_y_bogie(i+1) = v_y_bogie(i) + ay_bogie(i)*delta;
v_x_rc(i+1) = v_x_rc(i) + ax_rc(i)*delta;
v_y_rc(i+1) = v_y_rc(i) + ay_rc(i)*delta;
v_x_b(i+1) = v_x_b(i) + ab_x(i)*delta;
v_y_b(i+1) = v_y_b(i) + ab_y(i)*delta;
v_x_a(i+1) = v_x_a(i) + aa_x(i)*delta;
v_y_a(i+1) = v_y_a(i) + aa_y(i)*delta;
```

```
w1(i+1) = w1(i) + torque1(i)*delta -M_1(i)*delta;
w2(i+1) = w2(i) + torque2(i)*delta -M_2(i)*delta;
w3(i+1) = w3(i) + torque3(i)*delta -M_3(i)*delta;

omega_bogie(i+1) = omega_bogie(i)+alpha_bogie(i)*delta;
omega_rc(i+1) = omega_rc(i)+alpha_rc(i)*delta;

%% Performance Metrics Evaluation
% Power consumption
current1(i) = torque1(i)*stall_current/stall_torque;
current2(i) = torque2(i)*stall_current/stall_torque;
current3(i) = torque3(i)*stall_current/stall_torque;

p1(i) = abs(voltage*pwm1(i)/100*current1(i));
p2(i) = abs(voltage*pwm2(i)/100*current2(i));
p3(i) = abs(voltage*pwm3(i)/100*current3(i));

%Effective ground pressure
egp1(i) = F_n1(i)/(r*b);
egp2(i) = F_n2(i)/(r*b);
egp3(i) = F_n3(i)/(r*b);

%% Update Rocker bogie configuration

x1(i+1) = x1(i)+v1_x(i) * delta + 0.5*a1_x(i)*delta^2;
y1(i+1) = y1(i)+v1_y(i)*delta + 0.5*a1_y(i)*delta^2;

x2(i+1) = x2(i)+v2_x(i) * delta + 0.5*a2_x(i)*delta^2;
y2(i+1) = y2(i)+v2_y(i)*delta + 0.5*a2_y(i)*delta^2;

x3(i+1) = x3(i)+v3_x(i) * delta + 0.5*a3_x(i)*delta^2;
y3(i+1) = y3(i)+v3_y(i)*delta + 0.5*a3_y(i)*delta^2;

xb(i+1) = xb(i)+v_x_b(i) * delta + 0.5*ab_x(i)*delta^2;
yb(i+1) = yb(i)+v_y_b(i) * delta + 0.5*ab_y(i)*delta^2;

xa(i+1) = xa(i)+v_x_a(i) * delta + 0.5*aa_x(i)*delta^2;
ya(i+1) = ya(i)+v_y_a(i) * delta + 0.5*aa_y(i)*delta^2;

alpha1(i+1) = atan((ya(i+1)-y3(i+1))/(x3(i+1)-xa(i+1))); %rocker angle
alpha2(i+1) = atan((yb(i+1)-y2(i+1))/(x3(i+1)-xb(i+1))); %bogie angle
pitch(i+1) = alpha1_initial-alpha1(i+1);

pwm1(i+1) = pwm1(i);
pwm2(i+1) = pwm2(i);
pwm3(i+1) = pwm3(i);


%% Plot Rocker bogie configuration
hold off;
axis([-1 5 -1 5])
line([x1(i+1) xb(i+1)],[y1(i+1) yb(i+1)])
line([xb(i+1) x2(i+1)],[yb(i+1) y2(i+1)])
line([xb(i+1) xa(i+1)],[yb(i+1) ya(i+1)])
```

```
line([xa(i+1) x3(i+1)],[ya(i+1) y3(i+1)])
rectangle('Position',[x1(i+1)-r,y1(i+1)-r,2*r,2*r],'Curvature',[1,1])
rectangle('Position',[x2(i+1)-r,y2(i+1)-r,2*r,2*r],'Curvature',[1,1])
rectangle('Position',[x3(i+1)-r,y3(i+1)-r,2*r,2*r],'Curvature',[1,1])
drawnow
i=i+1
end
```

```
function [ x_cg_bogie, y_cg_bogie, x_cg_rocker, y_cg_rocker, x_cg_chassis,↙
y_cg_chassis, x_cg_rc, y_cg_rc, x_cg, y_cg ] = cg_calculator( x1,y1,x2,y2,x3,y3,xa,ya,↙
xb,yb,rchassis,alpha3,pitch,w_m,w_r1,w_r2,w_r3,w_r4,w_rocker,w_bogie,w_chassis,w_total)
%This function calculates the center of mass of each part of the rocker
%bogie system


    x_cg_bogie = (w_m*x1 +w_m*x2 + w_r1*(xb+x1)/2 + w_r2*(xb+x2)/2)/w_bogie;
    y_cg_bogie = (w_m*y1 +w_m*y2 + w_r1*(yb+y1)/2 + w_r2*(yb+y2)/2)/w_bogie;

    x_cg_rocker = (w_m*x3 + w_r3*(xa+xb)/2 + w_r4*(xa+x3)/2)/w_rocker;
    y_cg_rocker = (w_m*y3 + w_r3*(ya+yb)/2 + w_r4*(ya+y3)/2)/w_rocker;

    x_cg_chassis = xa-rchassis*cos(alpha3+pitch);
    y_cg_chassis = ya-rchassis*sin(alpha3+pitch);

    x_cg = (w_bogie*x_cg_bogie + w_rocker*x_cg_rocker + w_chassis*x_cg_chassis)↙
/w_total;
    y_cg = (w_bogie*y_cg_bogie + w_rocker*y_cg_rocker + w_chassis*y_cg_chassis)↙
/w_total;

    x_cg_rc = (w_chassis*x_cg_chassis+w_rocker*x_cg_rocker)/(w_chassis+w_rocker);
    y_cg_rc = (w_chassis*y_cg_chassis+w_rocker*y_cg_rocker)/(w_chassis+w_rocker);


end
```

```
function [ F_n F_t M] = force_calculator(r,b,thetaf,thetar,thetam,n,kc,kphi,k,c,phi,s)
%This function calculates the forces on wheel from ground

sigma1 = @(theta) r.^n.*(kc/b +kphi).*(cos(theta)-cos(thetaf)).^n; %thetam to theraf
sigma2 = @(theta) r.^n.*(kc/b +kphi).*(cos(thetaf - ((theta-thetar)/(thetam-thetar)).*↙
(thetaf-thetam))-cos(thetaf)).^n; %thetar to thetam
a = @(theta) -r/k .* (thetaf - theta - (1-s).*(sin(thetaf)-sin(theta)));
tau1 = @(theta)(c+sigma1(theta).*tan(phi)).*(1-exp(a(theta)));
tau2 = @(theta)(c+sigma2(theta).*tan(phi)).*(1-exp(a(theta)));
F_t1 = @(theta) tau1(theta).*cos(theta)-sigma1(theta).*sin(theta);
F_t2 = @(theta) tau2(theta).*cos(theta)-sigma2(theta).*sin(theta);
F_n1 = @(theta) sigma1(theta).*cos(theta)+tau1(theta).*sin(theta);
F_n2 = @(theta) sigma2(theta).*cos(theta)+tau2(theta).*sin(theta);
M1 = @(theta) F_t1(theta).*r.*cos(theta)+F_n1(theta).*r.*sin(theta);
M2 = @(theta) F_t2(theta).*r.*cos(theta)+F_n2(theta).*r.*sin(theta);


if thetaf == 0 && thetar==0
    F_t = 0;
    F_n = 0;
    M = 0;

else
F_t = r*b*(quad(F_t1,thetam,thetaf)+quad(F_t2,thetar,thetam));
F_n = r*b*(quad(F_n1,thetam,thetaf)+quad(F_n2,thetar,thetam));
M = r*b*(quad(M1,thetam,thetaf)+quad(M2,thetar,thetam));

end



end
```

```
function [sinkage, thetar, thetam, thetaf ] = sinkage_calculator(Ground_x,Ground_y,↙
Wheel_x,Wheel_y, Wheel_center_x,Wheel_center_y, Wheel_radius,s)
%This function calulates the sinkage of wheel in given ground profile
%Rear contact angle and front contact angles are calculated from point of
%intersections


[X Y] = intersections(Ground_x,Ground_y,Wheel_x,Wheel_y);
if size(X) == [0,1]
     thetar = 0;
     thetaf = 0;
     thetam = 0;
     sinkage = 0;

 else
     thetar = atan((Wheel_center_x-X(1,1))/(-Wheel_center_y+Y(1,1)));
     thetaf = atan((Wheel_center_x-X(2,1))/(-Wheel_center_y + Y(2,1)));
     a0 = 0.4;
     a1 = 0.1;
     thetam = thetaf*(a0+a1*s);
     sinkage = Wheel_radius*(1-cos(thetaf));


end
end
```